Journal of Hydrology: Regional Studies 60 (2025) 102539

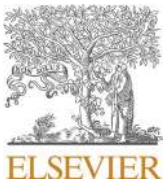

Contents lists available at ScienceDirect

Journal of Hydrology: Regional Studies

journal homepage: www.elsevier.com/locate/ejrh

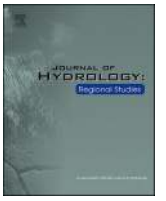

Unveiling four decades of spatiotemporal climate trends in Texas (1981–2023)

M.Shahriar Sonet [a], Yunuen Reygadas [b,*]

[a] School of Economic, Political and Policy Sciences, The University of Texas at Dallas, Dallas, TX, USA
[b] Department of Geosciences, Texas Tech University, Lubbock, TX, USA

ARTICLE INFO

Keywords:
Spatiotemporal Trends
Mann-Kendall Test
Theil-Sen Slope Estimator
PRISM, GridMET
Climate variability

ABSTRACT

Study Region: Texas, U.S.A.
Study Focus: Understanding climate variability is critical in Texas, a region influenced by moist air from the Gulf of Mexico and arid air from the Mexican Plateau. We investigated trends in annual and monthly mean temperature, total precipitation, and mean specific humidity, along with their monthly variability, from 1981 to 2023. We applied the modified Mann-Kendall test and Theil-Sen slope estimator to PRISM and GridMET 4-km datasets.
New Hydrological Insights for the Region: The most pronounced changes occurred during early summer, with Central Texas experiencing precipitation declines up to 125.27 mm and Far West Texas exhibiting temperature increases up to 3.68°C and humidity decreases up to 2.33 g/kg. A northwest–southeast gradient in humidity trends was observed, with declines across the Panhandle and increases near the Coast. Variability trends were more spatially and temporally extensive. Temperature variability increased from spring through fall by up to 1.19°C, particularly in Far West Texas. Precipitation variability intensified in May, August, and September, with swings up to 320 mm, especially in Central, Eastern, and Southern Texas. Humidity variability peaked in July and August in North Central and East Texas (up to 0.63 g/kg), while South Texas showed consistent declines. This reveals a growing climatic divide between humid and arid regions and underscores the need for adjusting cropcalendars, upgrading stormwater-systems, and expanding irrigation-infrastructure.

1. Introduction

Climate change is of the utmost importance due to its significant impacts on different environmental factors, such as vegetation cover, water availability, glacier retreat, sea level rise, biodiversity, and ecosystem stability. Precipitation and temperature are the two fundamental elements of climate that serve as the primary determinants for classifying climate types, which in turn shape the interactions between Earth's atmosphere, ecosystems, and human systems. In addition to this, atmospheric moisture plays a critical role in regulating energy balance and hydrological processes, further influencing these interactions. Unlike relative humidity, specific humidity is less dependent on temperature and provides a more direct and consistent measure of moisture in the lower atmosphere. Dry regions are especially vulnerable to changes in rainfall, temperature, and atmospheric moisture. Modifications in these patterns can disturb ecosystems, undermine agricultural output, and burden water resources, including aquifer recharge and groundwater

* Corresponding author.
E-mail address: yreygadas@ttu.edu (Y. Reygadas).

https://doi.org/10.1016/j.ejrh.2025.102539
Received 31 December 2024; Received in revised form 29 May 2025; Accepted 16 June 2025
Available online 20 June 2025

availability, which are crucial for both human and natural systems (Bradley and Malstaff, 2004; Brussolo et al., 2022). Gaining a comprehensive understanding of the spatiotemporal patterns of rainfall, temperature, and humidity in dry regions located far from the coastline, and comparing them with those near the shore, is critically important for formulating adaptive strategies, implementing sustainable water management techniques, and enhancing resilience in light of changing environmental circumstances.

Drylands account for 40 % of the United States territory (Kimmel et al., 2016), with Texas being home to one of the nation's most prominent dry regions. This research focuses on the State of Texas, which covers 692,000 km^2 and stretches across nearly eleven degrees of latitude and over thirteen degrees of longitude, fostering highly variable climate conditions (Dixon and Moore, 2011; North, 1995a, 1995b). Two primary factors contribute to Texas climatic variations: the movement of frontal systems from the northwest and the inflow of moist air from the Gulf of Mexico (Dixon and Moore, 2011; Hao and Singh, 2013; Li et al., 2019). Key geographical features facilitate these patterns: the central and eastern North American Cordillera acts as a barrier to east-west airflow, the Great Plains facilitate the rapid southward movement of cold air masses from the Arctic Circle to Texas, and the Gulf of Mexico acts as a moisture source, impacting humidity and moderating temperatures through its stable surface temperatures (Russell, 1945). Generally, Texas experiences an increasing mean temperature from north to south, with summers characterized by unpredictability in weather patterns (Blankenau et al., 2020; Kimmel et al., 2016; Meehl et al., 2000).

The impacts of changes in climate variables in Texas, including precipitation, humidity, and temperature, extend beyond the state borders, influencing ecosystems regionally. Significant spatiotemporal variations across climatically distinct regions underscore the interdependent nature of climate-related challenges (Ahmad et al., 2015; Hooshyar et al., 2020; Jiang and Yang, 2012). Detecting past trends and variability in climatic time series is essential for understanding potential future impacts (Some'e et al., 2012). As noted by Gocic and Trajkovic, (2013), Rajagopalan et al. (2009) and Sharma et al. (2016), global or continental observations are insufficient for local or regional planning purposes. Therefore, both local and regional analyses of historical trends are critical for accurate predictions and informed decision-making.

The availability of time series data, including temperature, humidity, and precipitation records, is vital for analyzing long-term trends in climate variables. Traditional data sources, such as rain gauge networks, provide precise point-based measurements but are spatially limited, leaving significant gaps in coverage, particularly in remote or sparsely populated areas. For a region like Texas, with its large geographic extent and climatic diversity ranging from arid drylands to humid coastal zones, these limitations pose challenges for accurately capturing spatial trends. Gridded climate datasets, such as those provided by Parameter-elevation Regressions on Independent Slopes Model (PRISM) and Gridded Surface Meteorological (GridMET), provide robust solutions to these challenges. Both datasets integrate surface station observations with advanced modeling and interpolation techniques to produce detailed and spatially consistent representations of precipitation, temperature, humidity, and other variables across diverse landscapes. PRISM further enhances its output by incorporating geographic features such as elevation, coastal proximity, and other local factors(Daly et al., 2021). Comparative studies, such as those by Neyestani et al. (2022) and Wolkeba and Mekonnen (2024) have evaluated the performance of various gridded datasets, finding GridMET and the Climate Prediction Center's unified gage-based precipitation dataset to be particularly reliable for climate analyses.

In trend detection, statistical techniques play a central role, with methods classified broadly into parametric and nonparametric. Parametric tests are often more powerful when their assumptions about data normality and independence are met; however, climatic data rarely meet these assumptions. Nonparametric methods, such as the Mann-Kendall (MK) trend test and Theil-Sen's slope (SS) estimator, are widely used for analyzing climatic and hydrological time series because they handle outliers more robustly and require fewer assumptions (Li, 2022; Mishra and Singh, 2010). Recent research has increasingly applied these methods to hydrological data, revealing significant trends in climate variables and enhancing the understanding of climatic dynamics over time (Liyew et al., 2024a; Liyew et al., 2024b; Reygadas et al., 2023; Schreiner-McGraw and Ajami, 2022; Wolkeba and Mekonnen, 2024).

Station-based analyses using the MK test and the SS estimator have provided valuable insights into climate trends, consistently identifying increases in temperature and varied precipitation patterns across different regions, such as the Lancang River in China (Yunling and Yiping, 2005), Saudi Arabia (El-Nesr et al., 2010), and Istanbul (Karaburun et al., 2011). In the United States of America, Statkewicz et al. (2021) identified a significant increase in extreme rainfall in Houston, Texas, highlighting the need for regional analyses of extreme climate events. However, as mentioned before, the spatial limitations of station-based data have led researchers to increasingly adopt gridded datasets while still relying on MK and SS methods. For example, Sharma et al. (2016) identified seasonal warming trends in eastern India using gridded datasets developed by the Indian Meteorological Department. Also in the United States, Sawyer and Stephen (2014) and Blankenau et al. (2020) used PRISM data to reveal increases in annual precipitation and minimum temperature in South Dakota and rising temperatures in the Big Pine Creek watershed, respectively. In Texas, Li (2022) found no significant trends in Texas over the last century but noted regional variations in temperature and precipitation patterns. Similarly, using Stage IV precipitation data from NEXRAD generated at the National Centre for Environmental Prediction (NCEP), Ghebreyesus and Sharif (2021) reported no significant trends in the monthly precipitation after 2013 in over 98 % of the state.

Regardless of the data type or analytical methods employed, research focused on Texas highlights spatial and seasonal differences in climate variables. For instance, Jiang and Yang (2012) and Sa'adi et al. (2019) investigated the impact of rising global temperatures on Texas precipitation, finding mixed trends depending on the location and time. Sa'adi et al. (2019) observed that downscaled global climate models from the World Climate Research Programme CMIP3 multi-model data predict significant surface air temperature rises by the end of the 21st century, particularly in northwest Texas, with ambiguous precipitation trends suggesting potential drying in many places. (Dixon and Moore (2011) analyzed seasonal and annual temperature and precipitation changes in Texas from 1932 to 2002, finding spatially non-uniform trends. Other studies have focused on specific meteorological station data in southeast Texas between 1991 and 2012, reveling both statistically significant rainfall trends and areas of no change Texas (Jiang and Yang, 2012; Sagarika et al., 2014).The influence of large-scale climatic phenomena such as the El Niño-Southern Oscillation (ENSO) and the Pacific

Decadal Oscillation (PDO) on Texas precipitation patterns has also been widely documented, with studies noting lagged correlations and spatial variability across the state (Ghebreyesus and Sharif, 2021).

These findings collectively emphasize the importance of continually improving the understanding of Texas's climatic variability and its broader implications for adaptation and policy development. Despite extensive research, several limitations remain. Studies on Texas's climate trends have predominantly focused on temperature and precipitation, with little to no attention given to humidity. Furthermore, many analyses have relied on station-based data, which, while valuable, often lacks the spatial resolution needed to capture finer-scale climate trends across Texas's diverse regions. Therefore, there is a need for studies that incorporate specific humidity alongside temperature and precipitation, using high-resolution gridded datasets to provide comprehensive understanding of spatial and temporal climate dynamics across Texas.

To address these knowledge gaps, this study investigates trends in annual and monthly mean temperature, total precipitation, and mean specific humidity, as well as their interannual variability at the monthly scale, across Texas from 1981 to 2023. These analyses are based on 4-km gridded datasets from PRISM and GridMET. The research seeks to answer the following question: How have temperature, precipitation, and specific humidity—along with their interannual variability at the monthly scale—changed across space and time in Texas from 1981 to 2023? From this question, three core hypotheses derive: Hypothesis 1) Given the interconnected nature of climate variables, trends in temperature, precipitation, and specific humidity are expected to exhibit spatial and seasonal alignment, with possible trade-offs between warming and moisture availability. Hypothesis 2) Because variability can respond more sensitively to short-term atmospheric dynamics than mean conditions, trends in interannual monthly variability are expected to reveal broader spatial and temporal patterns than trends in monthly means or totals. Hypothesis 3) Given the combination of strong solar forcing, increasing convective activity, and transitional atmospheric dynamics, early summer months are expected to exhibit the most pronounced and spatially extensive trends across variables. This research utilizes the modified MK and SS estimator to examine significant trends in these variables. This scientific approach aims to explain major patterns in climate variables, facilitating an understanding of the spatiotemporal distribution of climate changes in Texas. The findings offer insights into the state's climatic dynamics, supporting adaptation plans and guiding sustainable ground water management practices.

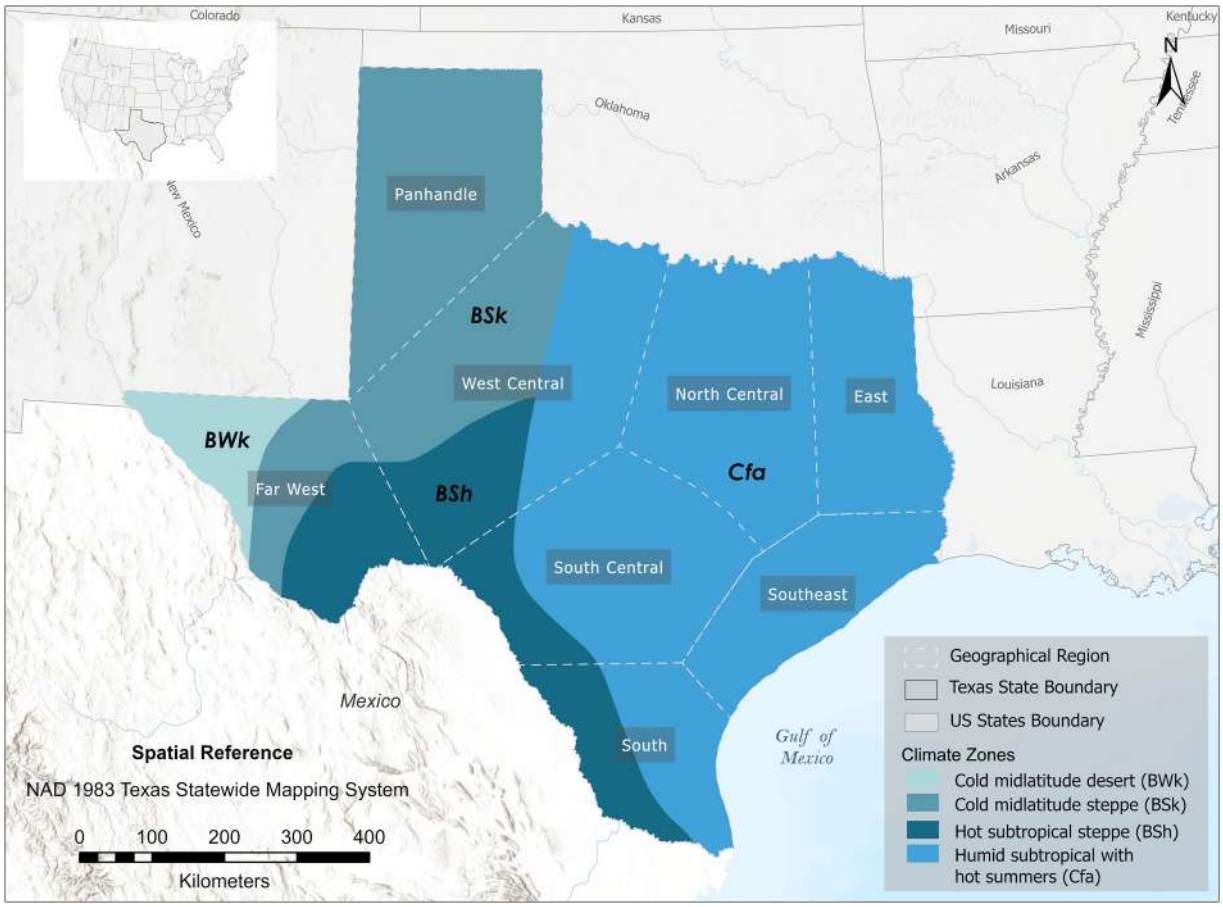

Fig. 1. Regions and climate zones in the study area. Climate boundaries are based on (Kottek et al., 2006) and regions on (Schmandt et al., 2011).

2. Study Area

Texas, the second-largest state in the United States, encounters a variety of weather patterns, with a wide range of temperatures and precipitation due to its broad geography (Dixon and Moore, 2011) (Fig. 1). Far West Texas experiences cold, arid winters and wet summers, driven by its basin and range topography; at higher elevations, precipitation is primarily influenced by moisture from the Gulf of Mexico. This moderate, humid air from the Gulf influences much of the state year-round, particularly the Southeast. During the summer months, substantial precipitation occurs due to the southeastward and southward Gulf breezes that encompass the entire state. Dry and extreme heat conditions often arise from the dryline, a boundary separating arid air from moist Gulf air, which is also frequently the source of supercell thunderstorms, especially in spring. The precise location of the dryline varies due to shifting circulation patterns. When moist Gulf air interacts with hot, arid air from the Mexican Plateau, a capping inversion can develop in Eastern Texas. With a frequency of approximately once per decade, this inversion induces periodic increases in temperature and decreases in dew points. As a result, Texas exhibits a wide range of climatic conditions, from humid coastal regions to arid deserts, influenced by the state's expansive topography and neighboring geographical elements (Sawyer and Stephen, 2014). More specifically, Texas can be divided into four major Köppen-Geiger climate types: humid subtropical with hot summers (Cfa), cold midlatitude desert (BWk), cold midlatitude steppe (BSk), and hot subtropical steppe (BSh) (Fig. 1).

According to previous investigations (North, 1995a, 1995b), Texas's climate exhibits considerable annual variability, which includes interannual to decadal fluctuations that can be partially linked to teleconnections with large-scale climate phenomena including the Pacific Decadal Oscillation (PDO), the North Atlantic Oscillation (NAO), and ENSO in the Equatorial Pacific (North, 1995a, 1995b; Watkins and O'Connell, 2006). These natural cycles and teleconnections lead to short-term fluctuations in temperature and precipitation, which overlay long-term patterns within time series, like those investigated in this study.

3. Data and methods

Trends derived from time series shorter than 30 years are highly influenced by the initial and final data points, making them inadequate for capturing long-term climate patterns or for estimating average conditions used in climate classification (Daly et al., 2021). To address this limitation, we conducted a four-decade geospatial analysis of annual and monthly mean temperature, total precipitation, and mean specific humidity, as well as their interannual monthly variability. The workflow includes: 1) data collection

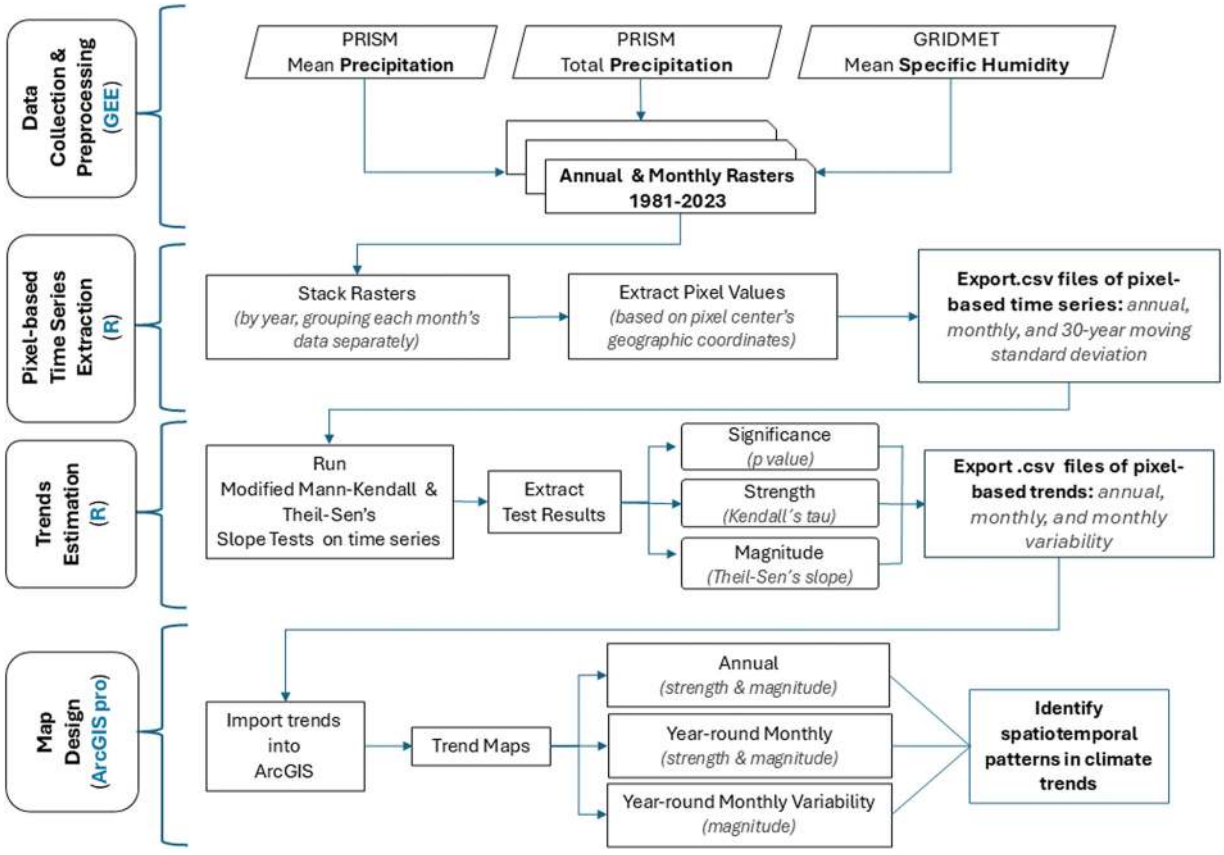

Fig. 2. Methodological workflow.

and preprocessing in Google Earth Engine (GEE), 2) extraction of pixel-based time series in R, 3) estimation of pixel-based trends in R, and 4) map design in ArcGIS Pro (Fig. 2).

3.1. Data acquisition and preprocessing

We used the GEE platform to calculate annual and monthly composites of total precipitation, mean specific humidity, and mean temperature across Texas from January 1981 to December 2023 (code available here). The variables were initially obtained on a daily basis from the ~4-km gridded datasets described below.

Precipitation and temperature data were obtained from the PRISM dataset, developed by the Oregon State University's PRISM Climate Group (Daly et al., 2015). PRISM incorporates station data from numerous networks across the United States and uses a physiographic interpolation method to generate high-resolution gridded climate data. This approach accounts for fluctuations in weather and climate influenced by elevation and other physiographic features. These include coastal influences, temperature inversions, and geographical barriers, such as those responsible for rain shadow effects. Daily PRISM retrievals span the contiguous United States and cover the period from January 1, 1981, to the present. PRISM prioritizes spatial precision by integrating all available station networks, even at the expense of temporal consistency (Abatzoglou, 2013; Daly et al., 2021). The original dataset provides daily totals of precipitation (including rain and melted snow) and mean temperature, calculated as the average of daily minimum and maximum temperatures (Table 1).

Specific humidity data were obtained from the University of Idaho's GridMET dataset (Russell, 1945). Specific humidity represents the mass of water vapor in the air relative to the total mass of air and is typically expressed in grams of water vapor per kilogram of air (g/kg). GridMET expands the capabilities of PRISM by integrating its high spatial resolution with the National Land Data Assimilation System (NLDAS) to provide additional climate variables, including specific humidity, wind speed, and solar radiation. Because GridMET is built on PRISM's spatial framework, it inherits its physiographic interpolation algorithm, which accounts for terrain and environmental features. This interpolation also ensures spatial completeness by filling gaps in observational data. Additional details of both the PRISM and GridMET datasets are presented in Table 1. PRISM and GridMET's spatial resolution and physiographic interpolation methods allow for detailed climate surface reconstruction. However, like any gridded product, they have known limitations. A more detailed discussion of those limitations is included in Section 5.2.

3.2. Pixel-based time series extraction

We extracted pixel-based time series from the annual and monthly rasters utilizing R 4.3.2 and RStudio 2023.12.1 (code available here). Raster file names were first organized into lists that grouped the data by month and/or year. For the monthly analysis, this organization facilitated the creation of twelve stackable objects, each corresponding to a specific month across the entire study period (e.g., stack 1: January 1981, January 1982, …, January 2023; stack 12: December 1981, December 1982, …, December 2023). Alongside this raster preparation, geographic coordinates (x and y) corresponding to the pixel centers were generated in ArcGIS Pro. These coordinates were transformed into a spatial points data frame, which enabled the extraction of raster values from each of the annual or monthly stacked objects based on their spatial locations. This process produced annual and monthly comma-separated values (.csv) files containing pixel-based time series organized by year (1981–2023) for each of the three variables. In addition, we derived a time series of standard deviation values using a 30-year moving window within each monthly dataset to assess variability.

3.3. Trends estimation

Trends were estimated in three different ways: 1) annual, 2) monthly, and 3) based on monthly variability, calculated from the 30-year moving standard deviations. Using R and R Studio, we applied the modified MK and the SS estimator (Kendall, 1948; Theil, 1950) to identify significant trends within the pixel-based time series and estimate their slopes (code available here). These statistical methods are well-suited for environmental and climatic data analysis (Li, 2022) as they provide robust measures even in the presence of missing data or seasonality. The non-parametric MK test assesses whether there is a statistically significant monotonic upward or downward trend on the variable of interest over time. The modified MK test extends the standard MK test by accounting for autocorrelation in the data series using the variance correction approach proposed by (Hamed and Rao, 1998). The modified MK identifies

Table 1
Source data characteristics. ppt = precipitation, tmean= mean temperature, sph = specific humidity. * Estimated minimum or maximum values. Source: (Abatzoglou, 2013; Daly et al#, 2015).

Dataset	Spatial resolution	Band	Unit	Min value	Max value	Description
PRISM Oregon State University's Daily Spatial Climate Dataset AN81d	4638.3 m	ppt	mm	0*	731.65*	Daily total precipitation *(including rain & melted snow)*
		tmean	°C	−40.37*	45.98*	Daily mean temperature *(calculated as (tmin+tmax)/2)*
GridMET University of Idaho Gridded Surface Meteorological Dataset	4638.3 m	sph	g/kg (mass fraction)	0*	0.02*	Specific humidity *(mass of water vapor in the air relative to the total mass of air)*

significant monotonic trends and evaluates their strength using the Kendall's Tau (τ) correlation coefficient. Kendall's Tau ranges from −1 (i.e., consistently decreasing trend) to + 1 (i.e., consistently increasing trend).

While the modified MK test evaluates the presence and strength of trends, it does not measure their magnitude (i.e., the extent of the changes). To quantify the magnitude of trends, we employed the non-parametric SS estimator. This method calculates the rate of change based on the time frequency of the time series and can also be used to determine the absolute change over the study period. SS is particularly effective for climatic data where serial correlation is common. The SS estimator computes the median slope among all pairs of data points, providing a robust measure of trend magnitude that is less sensitive to outliers and skewed data distributions. From the application of the tests described above, three key statistics were extracted to characterize trends in the time series data:

- Significance (p-value): determines whether the observed trend is statistically significant. Trends were considered significant when the p-value was below 0.05.
- Strength (Kendall's Tau, τ): measures the strength of the monotonic relationship, representing how consistently the trend increases or decreases over time. Trends can range from strongly decreasing (τ=−1) to strongly increasing (τ=+1).
- Magnitude (Theil-Sen's slope): quantifies the rate of change in the time series, indicating how much a trend increases or decreases per unit of time. The range of values is determined by the variable's units of measurement. For the annual and monthly trend analyses, the year-to-year slope was multiplied by 43 to represent the total change over the 1981–2023 period. For monthly variability trend, which were derived from 30-year moving standard deviations, the slope was multiplied by 14 (the number of resulting windows) to estimate the overall change in variability across the study period.

Each pixel's time series was analyzed to retrieve these key metrics, providing insights into the nature and significance of trends across the spatial domain. The *'modifiedmk'* package was used to apply the modified MK test together with the SS estimator. The results from this trend analysis were then compiled into.csv files containing each pixel's time series ID, geographic coordinates, p value, strength, magnitude, and qualitative category (i.e., positive, negative, or not significant).

Regarding anomalous values, while we did not apply a separate outlier detection method before conducting the statistical analyses, the SS estimator handles well outliers when estimating the trend magnitude, as it computes the median of all possible pairwise slopes, which minimizes the influence of extreme values compared to mean-based estimators. The Modified MK test specifically addresses autocorrelation, which does not directly mitigate the influence of anomalous values. However, the combination of the Modified MK test and the SS estimator provides a reliable framework for trend detection, even in the presence of some anomalous values.

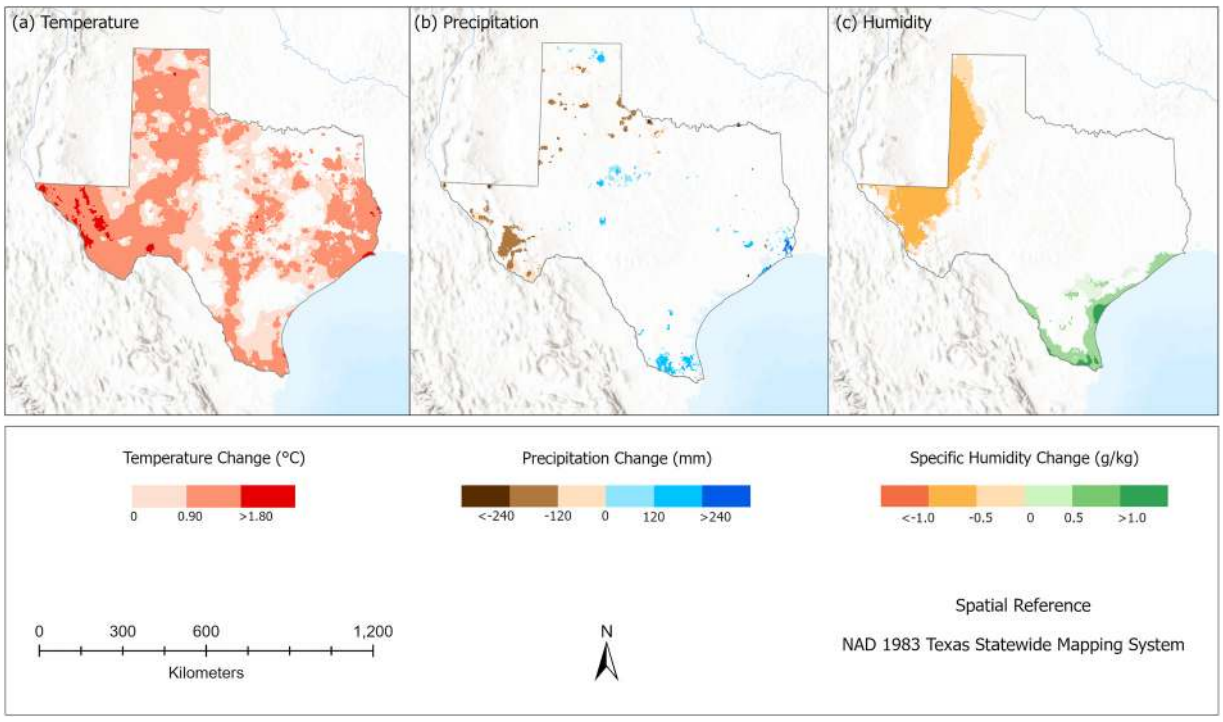

Fig. 3. Annual trend magnitudes of (a) mean temperature, (b) total precipitation, and (c) mean specific humidity. Only significant trends ($p < 0.05$) are displayed.

3.4. Map design

Trend analysis results stored in.csv files were imported into ArcGIS Pro to spatially analyze changes over time. Geographic coordinates were projected to NAD 1983 Texas Statewide Mapping System to ensure spatial accuracy. Based on these projected coordinates, we generated maps of annual, year-round monthly, and year-round monthly variability trends for each of the three variables. Due to an observed skewness in the data towards trends of low strengths, the trend's strength (Kendall's Tau) for all variables was manually reclassified into the three following classes: |0–0.15, 0.15–0.30, 0.30–1.00|. Similarly, the magnitude of each variable (expressed in ° C, mm, and g/kg for temperature, precipitation and specific humidity, respectively) was reclassified into three classes using the geometric interval method, which is particularly well-suited for continuous environmental data that may be skewed or unevenly distributed, as was the case in our trend magnitude datasets. This method ensures a balanced distribution of values across each class range and maintains consistent intervals between them. The suitability of the geometric interval method for mapping environmental data has been demonstrated in previous studies (Hamed and Rao, 1998; Huan et al., 2012; Costache et al., 2020; Lu et al., 2021). Thus, these maps provide a comprehensive representation of the consistency of changes (trend strength) and the extent of those changes (trend magnitude).

4. Results

Overall annual trends of mean temperature, total precipitation, and mean specific humidity across Texas between 1981 and 2023 revealed distinct patterns of change. Annual temperature increased across most of the state, with particularly pronounced warming in Far West Texas, where temperature increases reached 2.65°C, with a Kendall's tau of 0.57, indicating a consistently increasing trend (Figs. 3a and 4a). Annual precipitation trends were less widespread, with positive trends covering limited areas in the Panhandle and Central, Southern, and Eastern regions of Texas, and negative trends observed in Far West and Northwest Texas. Increases in precipitation reached up to 350 mm in Eastern Texas with a Kendall's tau of only 0.15, while decreases reached up to - 300 mm with a Kendall's tau of 0.45 (Figs. 3b and 4b). Annual specific humidity displays a clustered pattern, with positive trends near the Southern coast and negative trends in the Western regions. Decreases in specific humidity reached up to – 0.96 g/kg in West Texas, with a Kendall's tau of 0.37, while increases near the Southern coast reached up to 1.40 g/kg, with a Kendall's tau of 0.43 (Figs. 3c and 4c).

At the monthly scale, mean temperature significant trends are predominantly positive, particularly during the summer and fall months. Notably, in June, more than two-thirds of the state exhibited increasing temperatures (Fig. 5a). For precipitation, positive trends are rare, with decreasing trends dominating significant changes, especially in late fall and winter, when at least 10 % of the state experienced reduced rainfall (Fig. 5b). For specific humidity, although positive trends are observed during the summer and early fall months, significant changes are largely negative, affecting up to one-quarter of the state in February (Fig. 5c). A detailed analysis of

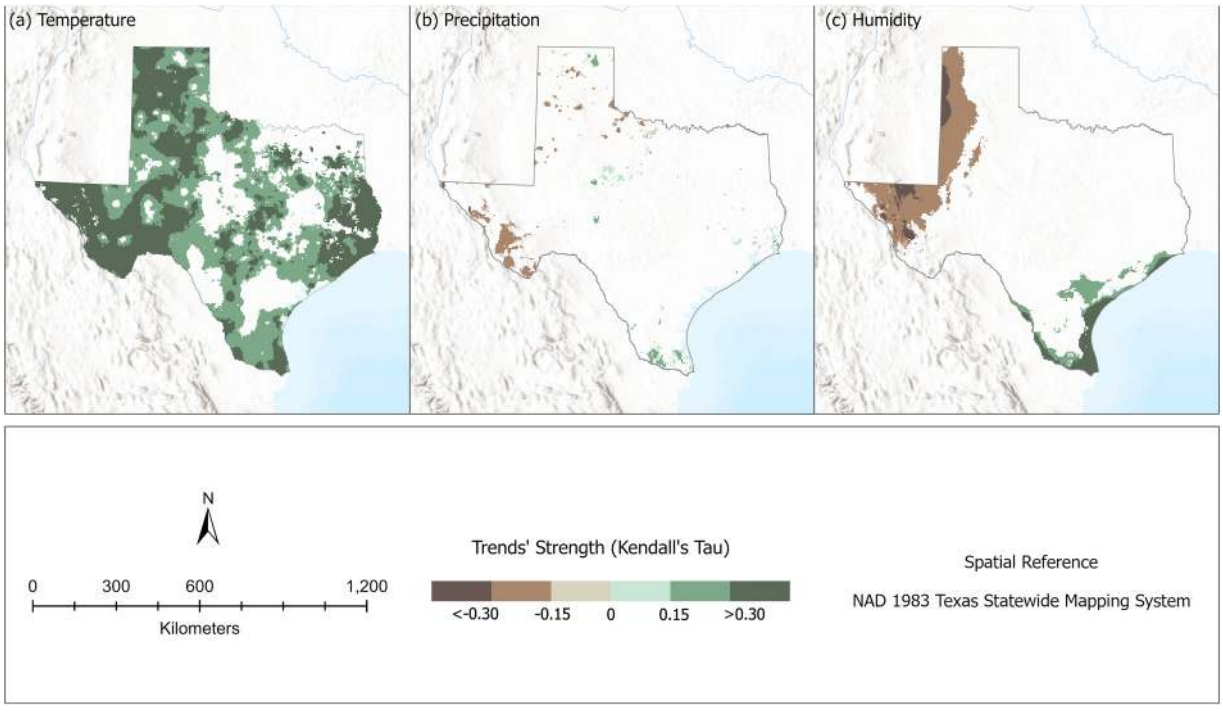

Fig. 4. Annual trend strengths of (a) mean temperature, (b) total precipitation, and (c) mean specific humidity. Only significant trends ($p < 0.05$) are displayed.

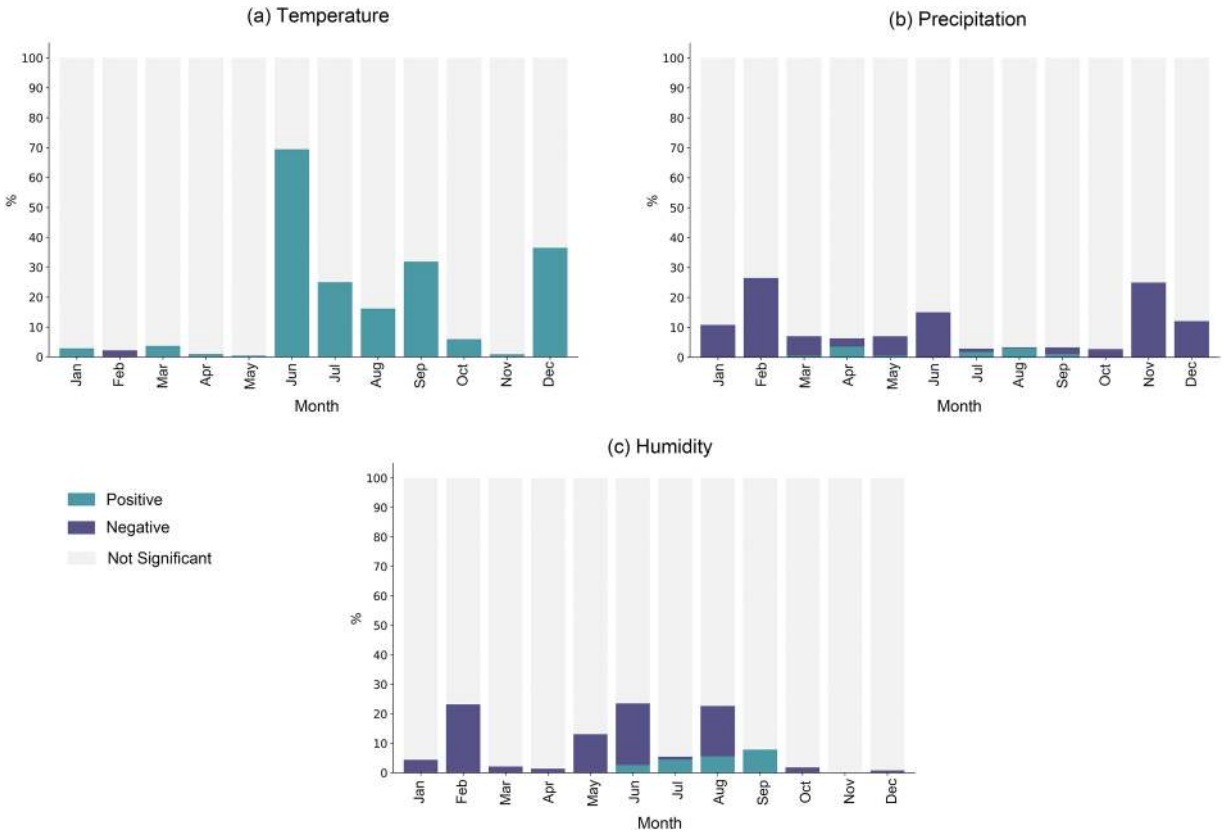

Fig. 5. Percentage distribution of significant ($p < 0.05$) and non-significant ($p \geq 0.05$) monthly trend direction for (a) mean temperature, (b) total precipitation and (c) mean specific humidity.

these monthly patterns is provided in the following sections.

4.1. Temperature

The observed spatial patterns (Figs. 6 and 7) and statistical distribution (Fig. 8) of temperature trends in Texas within the last four decades indicate a consistent warming throughout the year, with magnitudes ranging from 0.45°C to 3.68°C (Figs. 6 and 8a) and strengths from 0.05 to 0.48 Kendall's tau (Figs. 7 and 8b). Warming trends are more pronounced and consistent during early summer (June) and late fall (December), particularly over the western and northeastern regions of the state. February is the only month exhibiting a cluster of cooling trends, which occur over the eastern portion of the Panhandle with mostly moderate magnitudes (1.60–2.40°C) and weak strengths (< 0.15 Kendall's Tau).

Positive temperature trends exhibit greater statistical dispersion in both magnitude (Fig. 8a) and strength (Fig. 8b), as depicted by wider interquartile ranges (IQRs) and longer whiskers, especially from June to October and in December. Spatially, June and December show the largest extent of positive trends, particularly in Far West Texas, where magnitudes of change reach up to 3.68°C (Fig. 6) and strength up to 0.48 Kendall's tau (Fig. 7). In contrast, negative trends are less variable in both magnitude (Fig. 8a) and strength (Fig. 8b), are confined to a few months, and are much less widely distributed (Figs. 7 and 8). As aforementioned, cooling is concentrated in small northern areas during February, where changes are mostly moderate in magnitude (<-2.4°C) and weak in strength (<-0.15 Kendall's tau).

Positive magnitude has numerous outliers and are particularly high in June and December. These outliers highlight regions where temperature increases are significantly greater (from 3.00°C to 3.68°C) compared to the average magnitude (1.80°C in June and 2.11°C in December). Positive strength outliers for these same months are also abundant and indicate regions where changes of temperature are much more consistently increasing (from 0.30 to 0.48 Kendall's tau) compared to the average strength (0.26 Kendall's tau in June and 0.23 Kendall's tau in December). Negative trends, on the other hand, exhibit far fewer outliers, confirming that regions with cooling trends show less extreme behavior.

Overall, positive temperature trends are prevalent throughout the year, with generally larger magnitudes and stronger Kendall's tau values. However, temperature increases are non-uniform across regions, with some areas experiencing significantly larger increases and stronger trends than others. In contrast, negative trends are rare, more uniform, with smaller magnitudes and weaker strength, and they occur only in a few months.

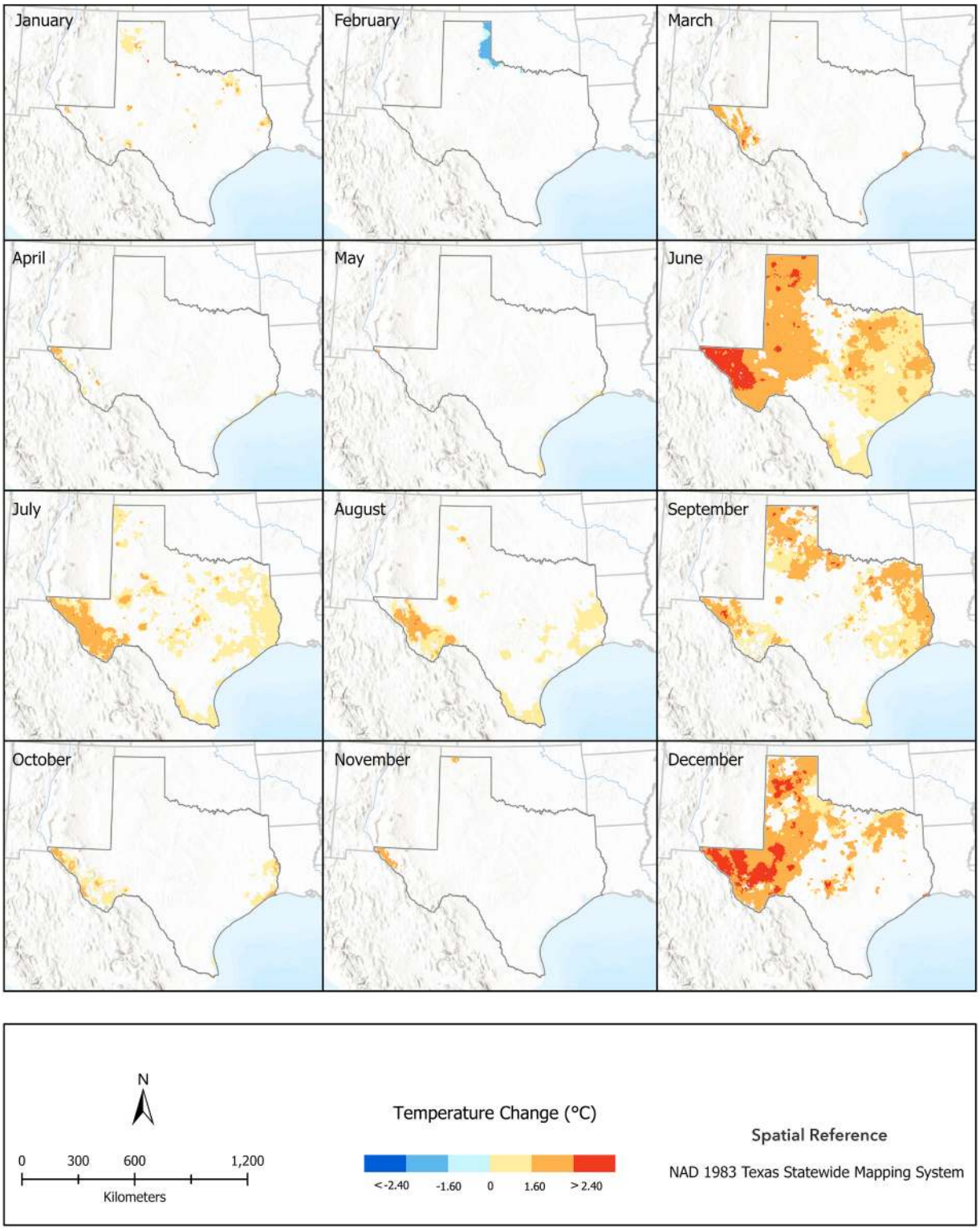

Fig. 6. Temperature trend's magnitude in Texas, 1981–2023. Only significant trends ($p < 0.05$) are displayed.

Regarding monthly variability, most months, except for December, January, and April, exhibit increasing trends, which suggests that temperature is becoming more variable and less predictable in much of Texas (Fig. 9). Extreme fluctuations are observed in June in Far West Texas, where temperature variability increases up to 1.19 °C. November shows widespread increases in variability across

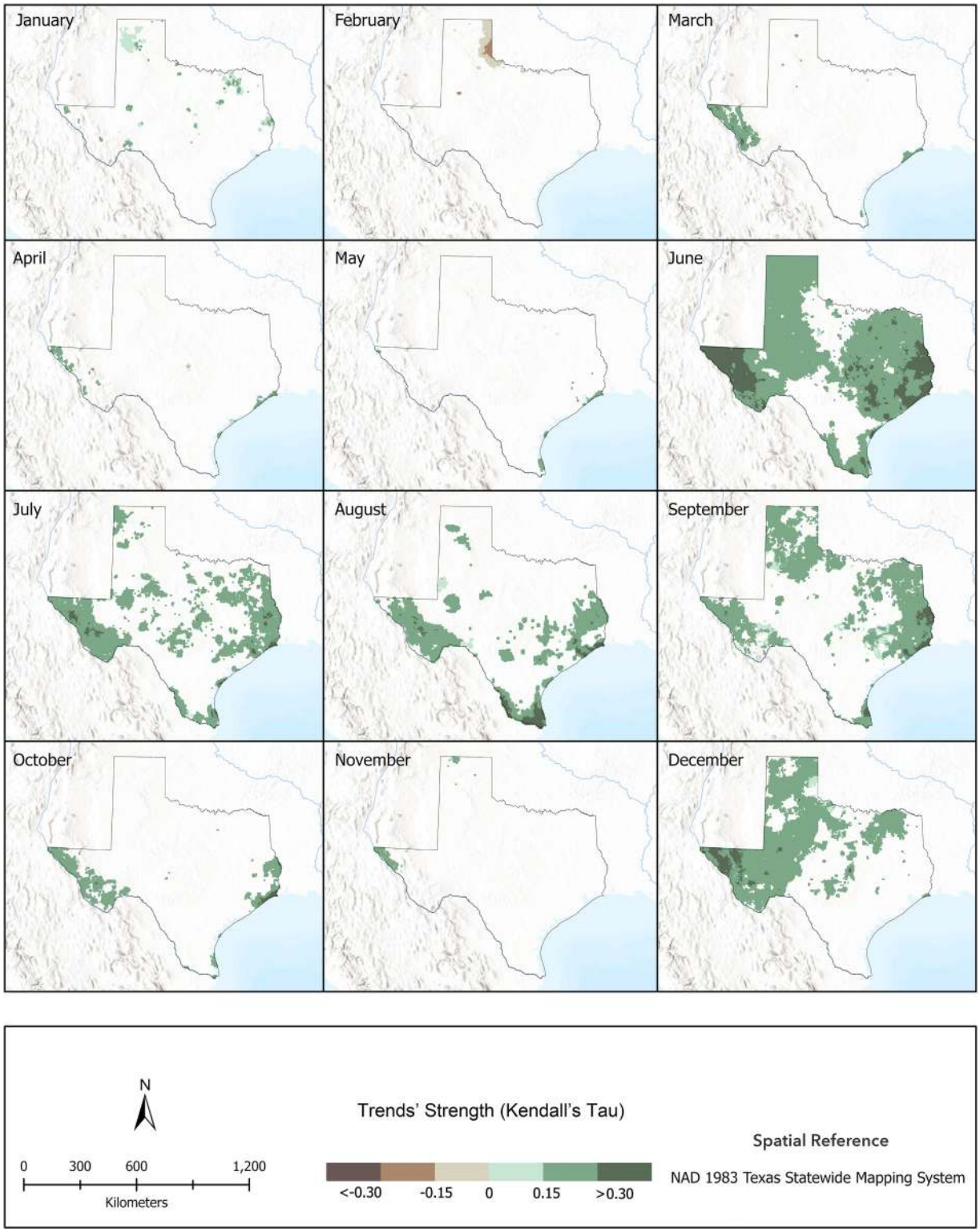

Fig. 7. Temperature trend's strength in Texas, 1981–2023. Only significant trends ($p < 0.05$) are displayed.

nearly the entire state, in contrast to January, when most of Texas displays a trend toward more stable temperatures, with year-to-year differences becoming smaller. These results highlight a general pattern of increasing temperature variability from spring through fall, with relative stability during early winter.

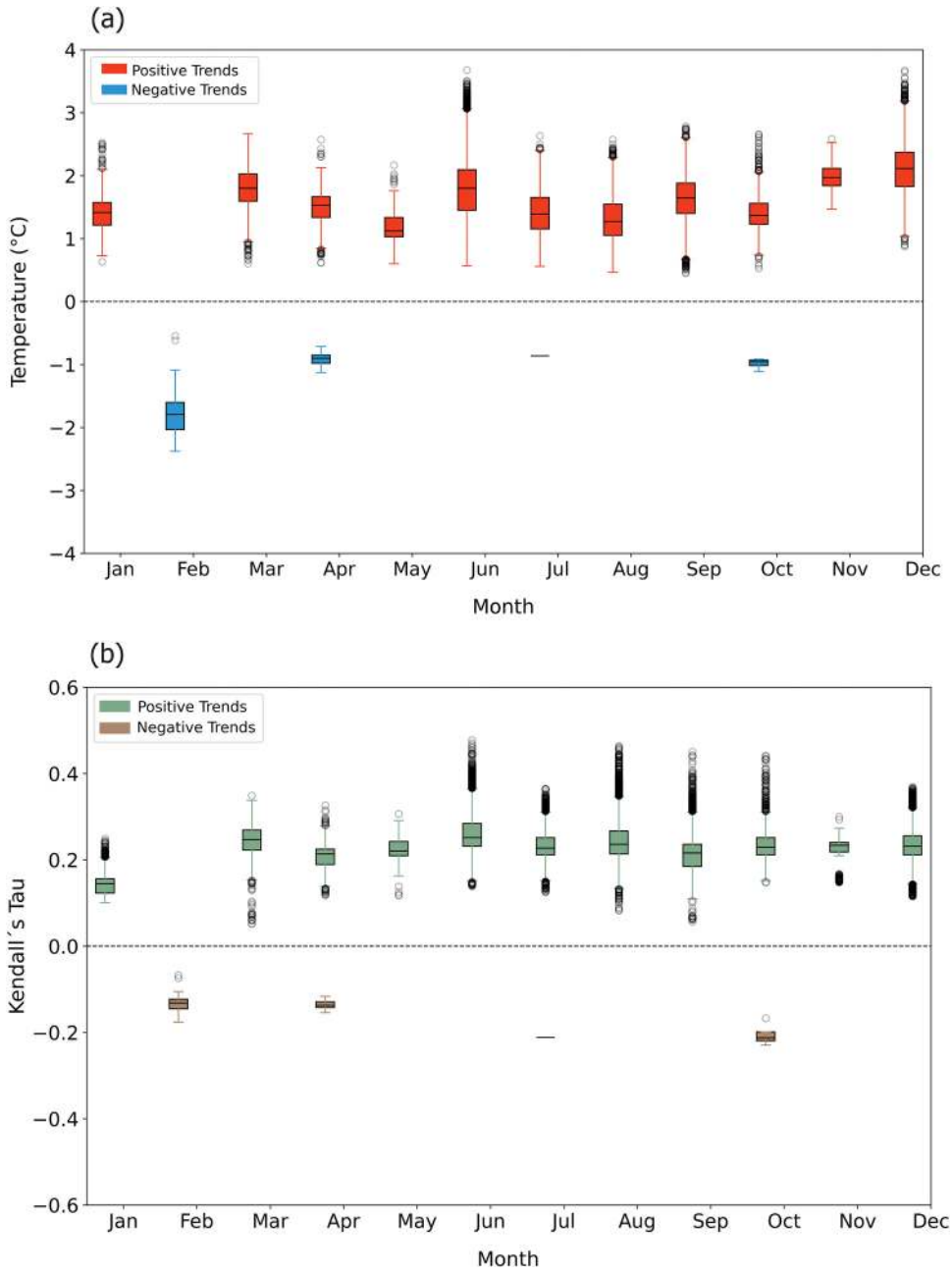

Fig. 8. Monthly (a) magnitude and (b) strength of temperature trends. Outliers are defined as values falling outside 1.5 times the interquartile range below Q1 or above Q3. See supplementary material, section A, for examples of extreme trends.

4.2. Precipitation

The spatial patterns (Figs. 10 and 11) and statistical distribution (Fig. 12) of precipitation trends across Texas in the last four decades suggest a consistent drying trend, with magnitudes ranging from –6 mm to –125 mm (Figs. 10 and 11a) and strengths from −0.05 to −0.41 Kendall's Tau (Figs. 11 and 12b). Although occurring with less frequency, positive trends are also present, particularly during the warmer months (April to September), where they show greater statistical dispersion in both magnitude (2 mm to 116 mm) and strength (0.02–0.36 Kendall's Tau).

Decreasing rainfall trends are particularly evident in February, June, November, and December, with these months generally showing greater variation in both magnitude and strength. February exhibits a cluster of negative trends over South and Southeastern Texas, with mostly moderate magnitudes (up to –99 mm) and moderate to strong strengths (up to –0.41 Kendall's Tau). June registered the highest negative outlier (–125.27 mm) over Central Texas, but excluding outliers, the typical range of positive trends for this month

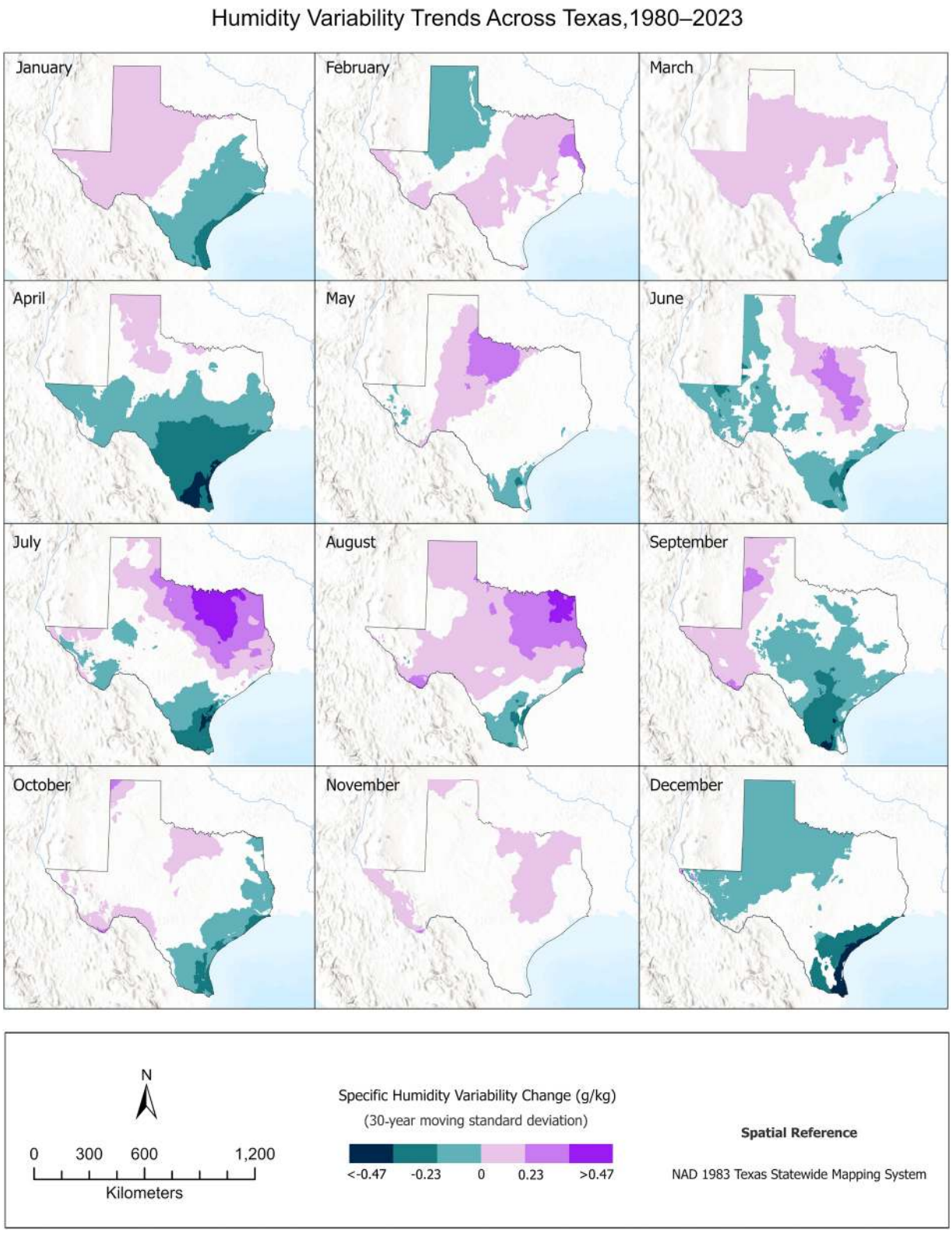

Fig. 9. Cumulative temperature variability changes across Texas from 1981 to 2023, based on trends in 30-year moving standard deviations of monthly mean temperature. Only significant trends ($p < 0.05$) are displayed.

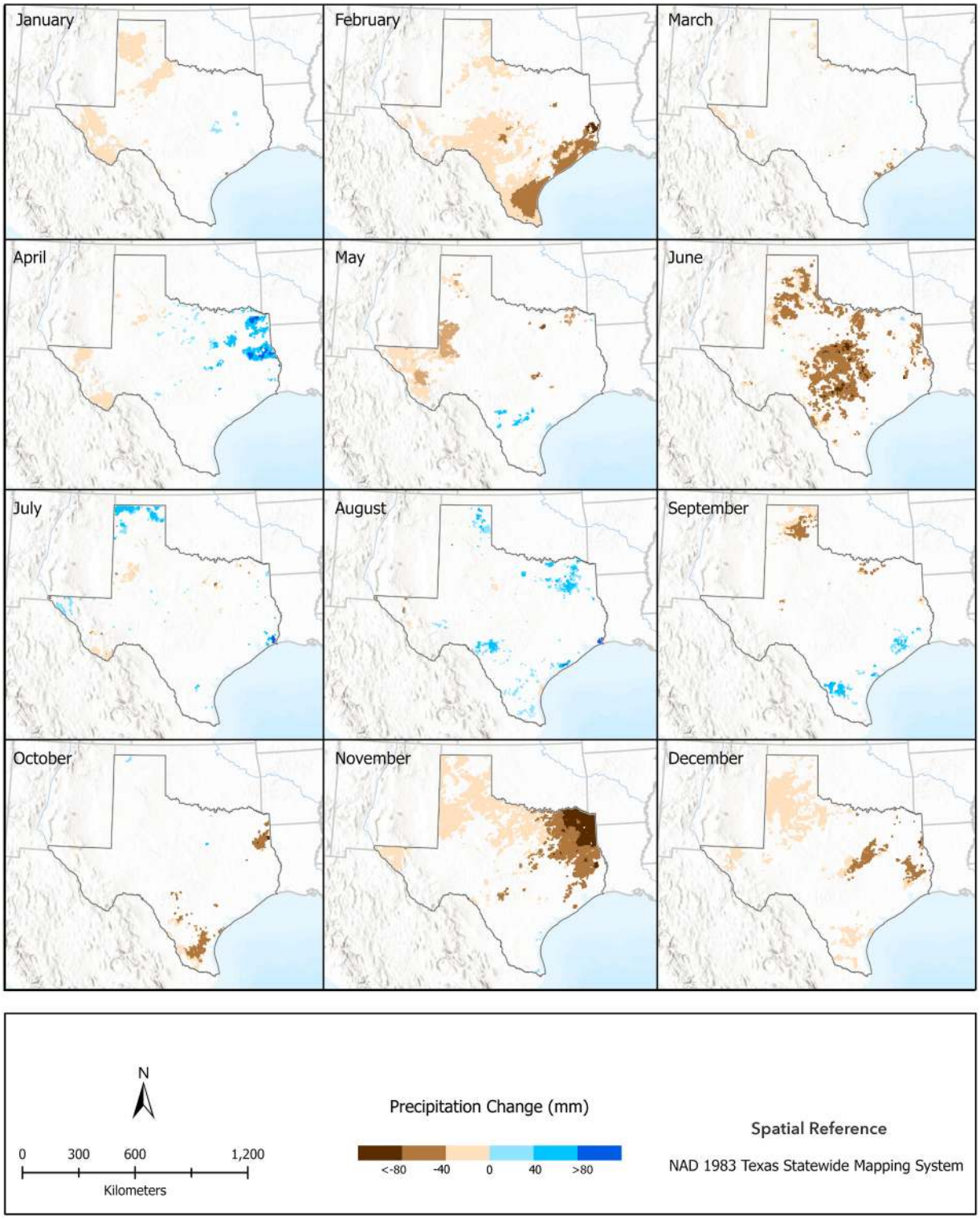

Fig. 10. Precipitation trend's magnitude in Texas, 1981–2023. Only significant trends ($p < 0.05$) are displayed.

falls between 17.65 mm and 22.30 mm. November shows intense drying in East Texas, with trends displaying high magnitudes (–120 mm to –80 mm) and moderate strengths (–0.15 to –0.30 Kendall's Tau), along with the greatest statistical dispersion in precipitation decrease, but no outliers. On the other hand, April displays the least statistical dispersion in precipitation magnitude but in

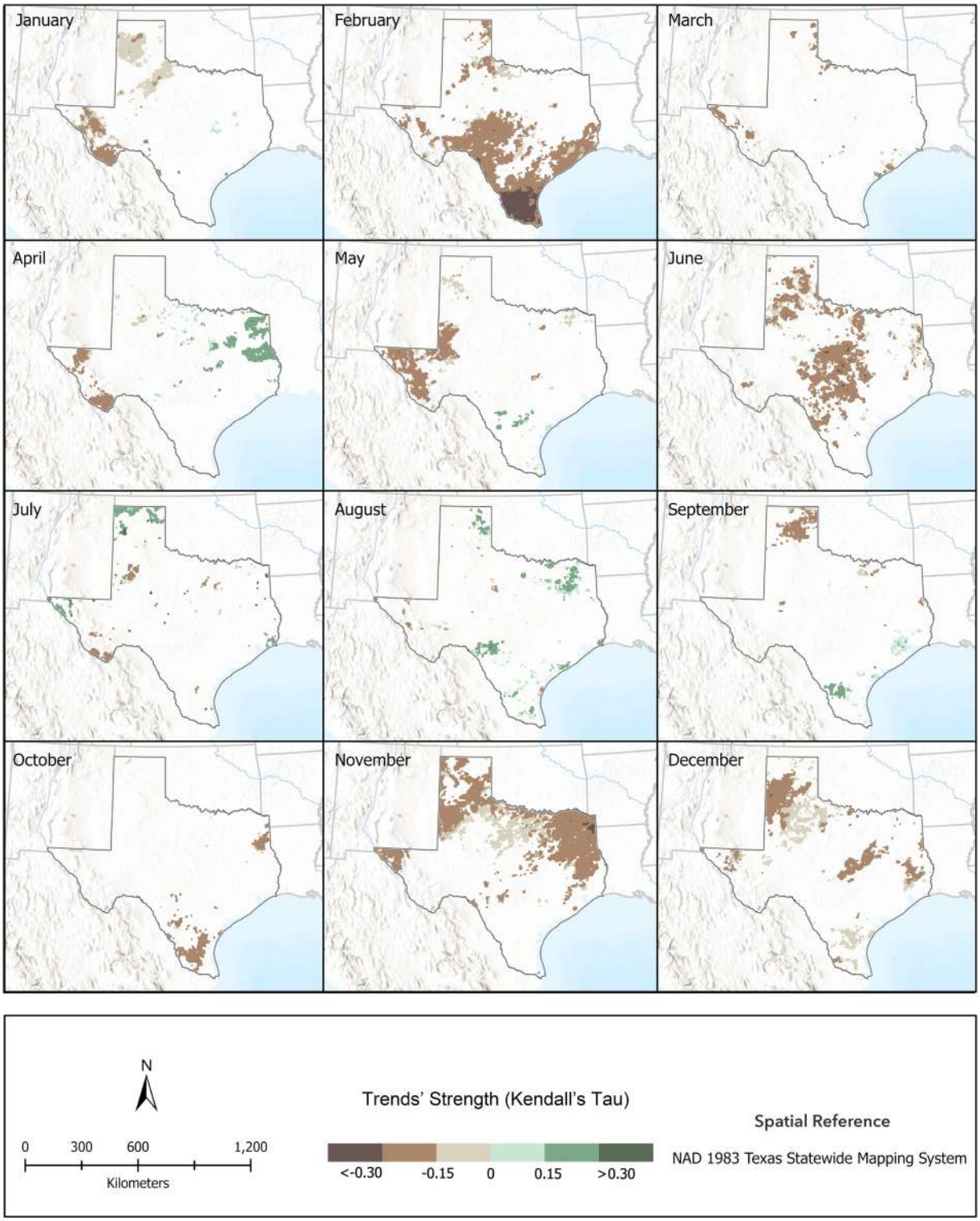

Fig. 11. Precipitation trend's strength in Texas, 1981–2023. Only significant trends ($p < 0.05$) are displayed.

East Texas, where high magnitudes (up to –120 mm) and moderate strengths (0.15–0.30 Kendall's Tau) are observed.

Regions experiencing drying trends generally show more uniform patterns in both magnitude (Fig. 12a) and strength (Fig. 12b). However, February, June, and November exhibit significant statistical dispersion with extreme drying trends, as evidenced by wider

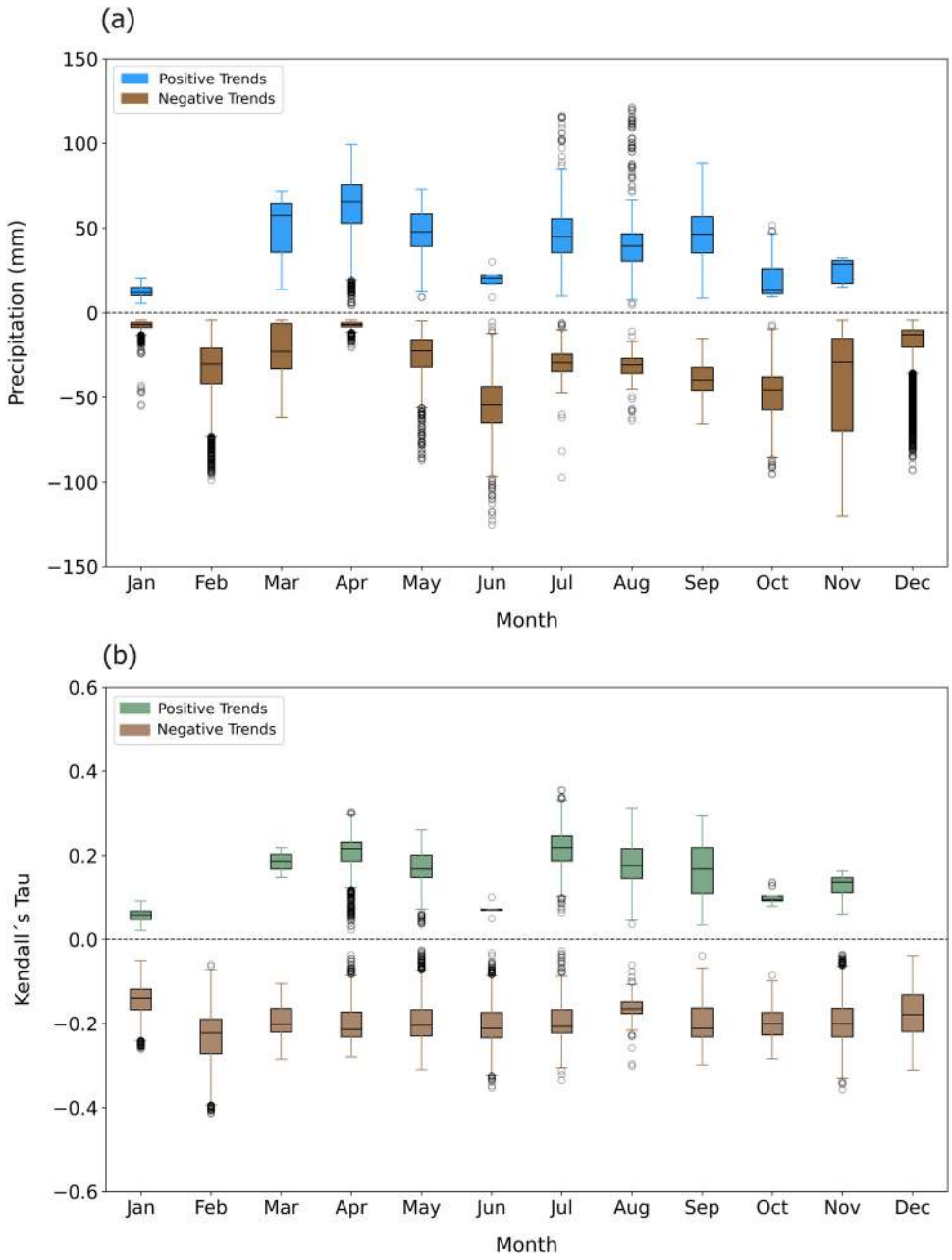

Fig. 12. Monthly (a) magnitude and (b) strength of precipitation trends. Outliers are defined as values falling outside 1.5 times the interquartile range below Q1 or above Q3. See supplementary material, section A, for examples of extreme trends.

IQRs, long whiskers and numerous outliers. The median magnitude values are particularly low in June, which indicates a considerable reduction in precipitation in late spring. Positive trends are less widely distributed as observed in Figs. 10 and 11, but they show greater statistical dispersion in both magnitude and strength, particularly during the warmer months. The prominent outliers in the trends' magnitude of July and August suggest that some areas experience much larger increases in rainfall than others in those two months. Overall, drying trends are widespread and more uniform across Texas, while positive trends are less frequent, highly variable, and more spatially concentrated during the warmer months.

Precipitation monthly variability displays heterogeneous spatial and temporal patterns, with marked increases during several months, indicative of more frequent wet–dry extremes (Fig. 13). May, August, and September exhibited the largest cumulative increases in variability, reaching up to 320 mm, which suggests more erratic and less predictable rainfall patterns. These fluctuations, which complicate the detection of long-term trends, were most pronounced in Central, Eastern, and Southern Texas. Other months also showed areas with increasing variability, though with smaller magnitudes and generally more localized patterns. In contrast, February,

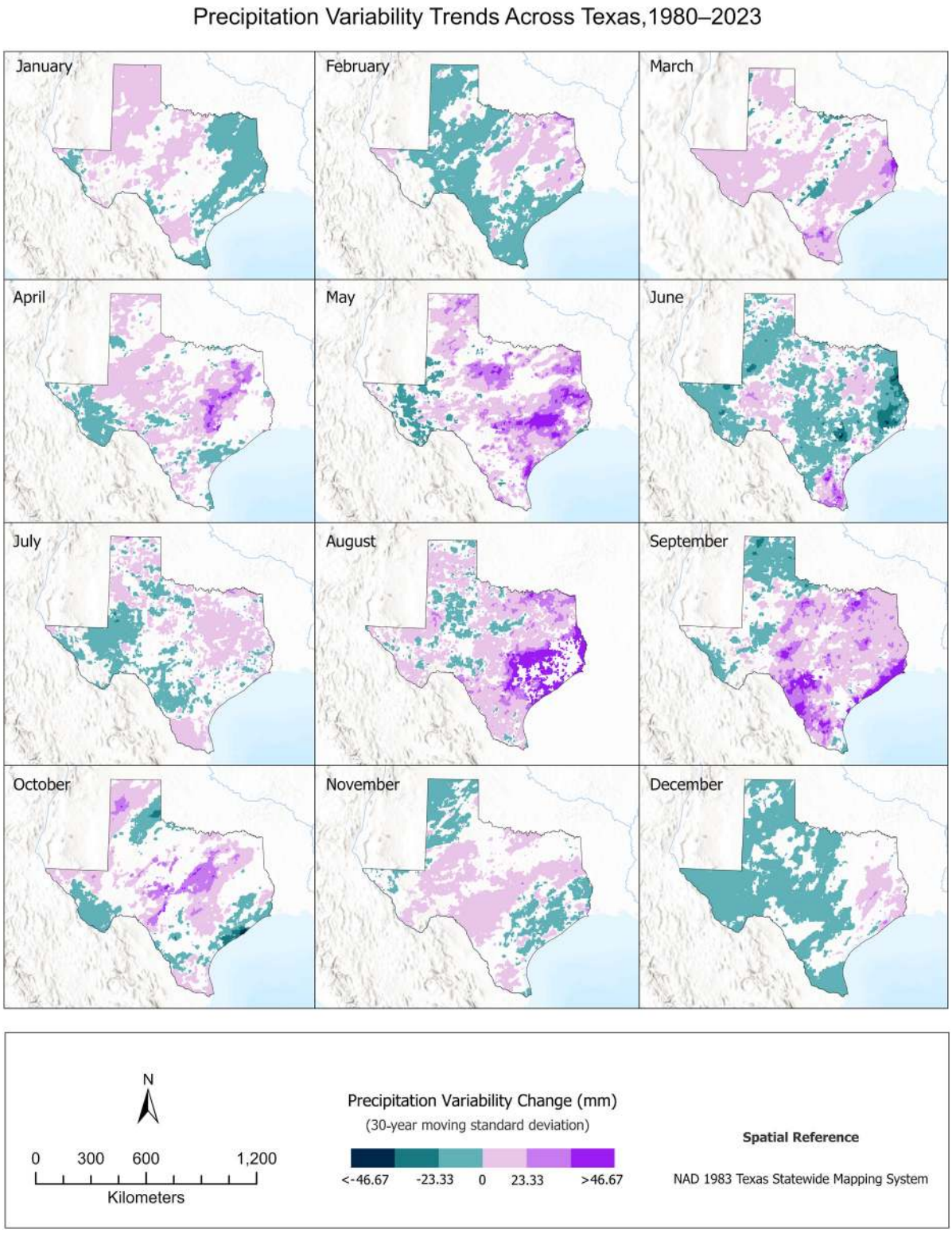

Fig. 13. Cumulative precipitation variability changes across Texas from 1981 to 2023, based on trends in 30-year moving standard deviations of monthly total precipitation. Only significant trends ($p < 0.05$) are displayed.

June, and December exhibited widespread areas of decreasing variability, with negative trends of up to –68 mm, particularly across East Texas. These reductions in variability may indicate a shift toward more consistent and uniform precipitation patterns during these months. All months displayed mixed patterns, with adjacent regions experiencing opposing trends in precipitation variability. This

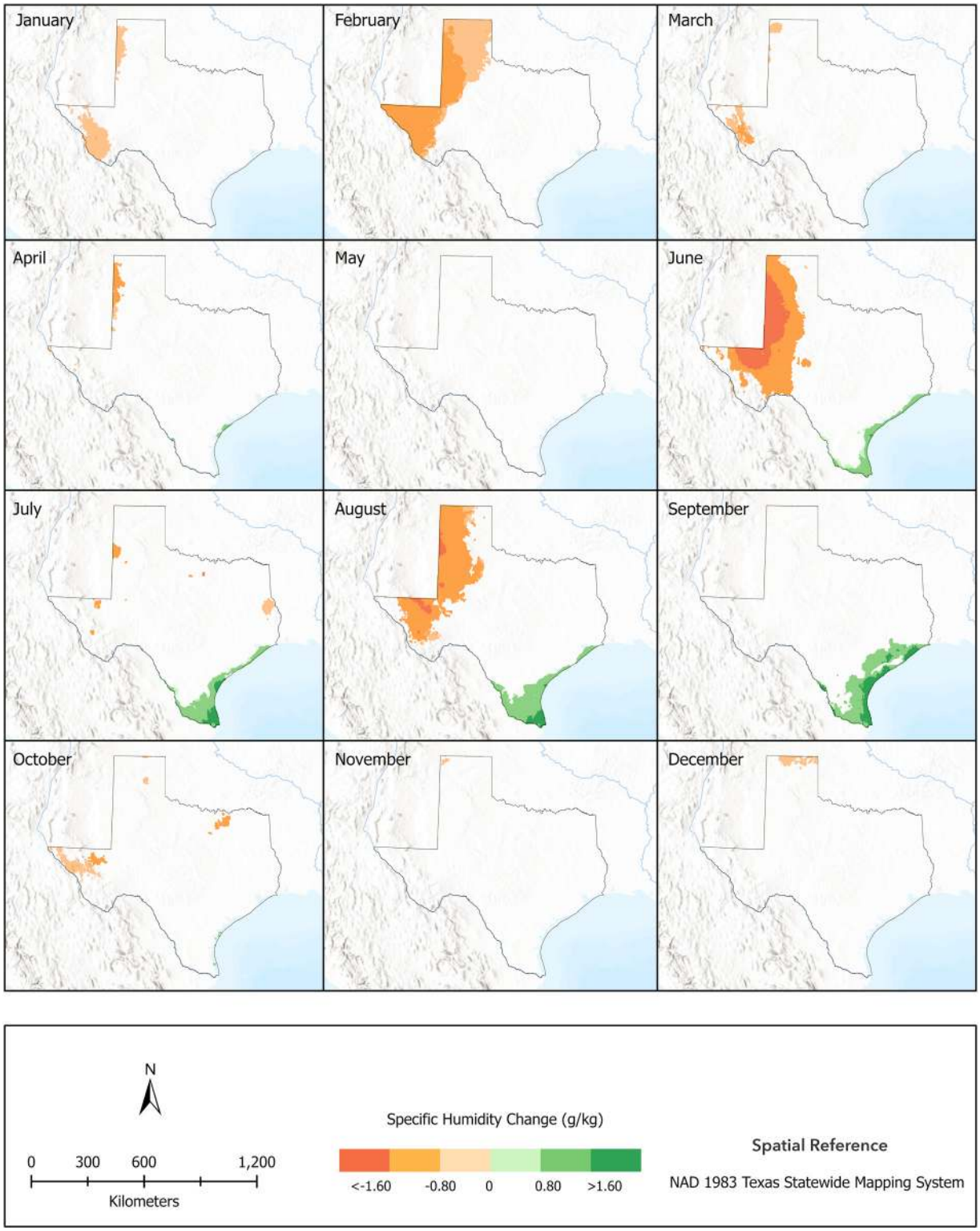

Fig. 14. Specific Humidity trend's magnitude in Texas, 1981–2023. Only significant trends ($p < 0.05$) are displayed.

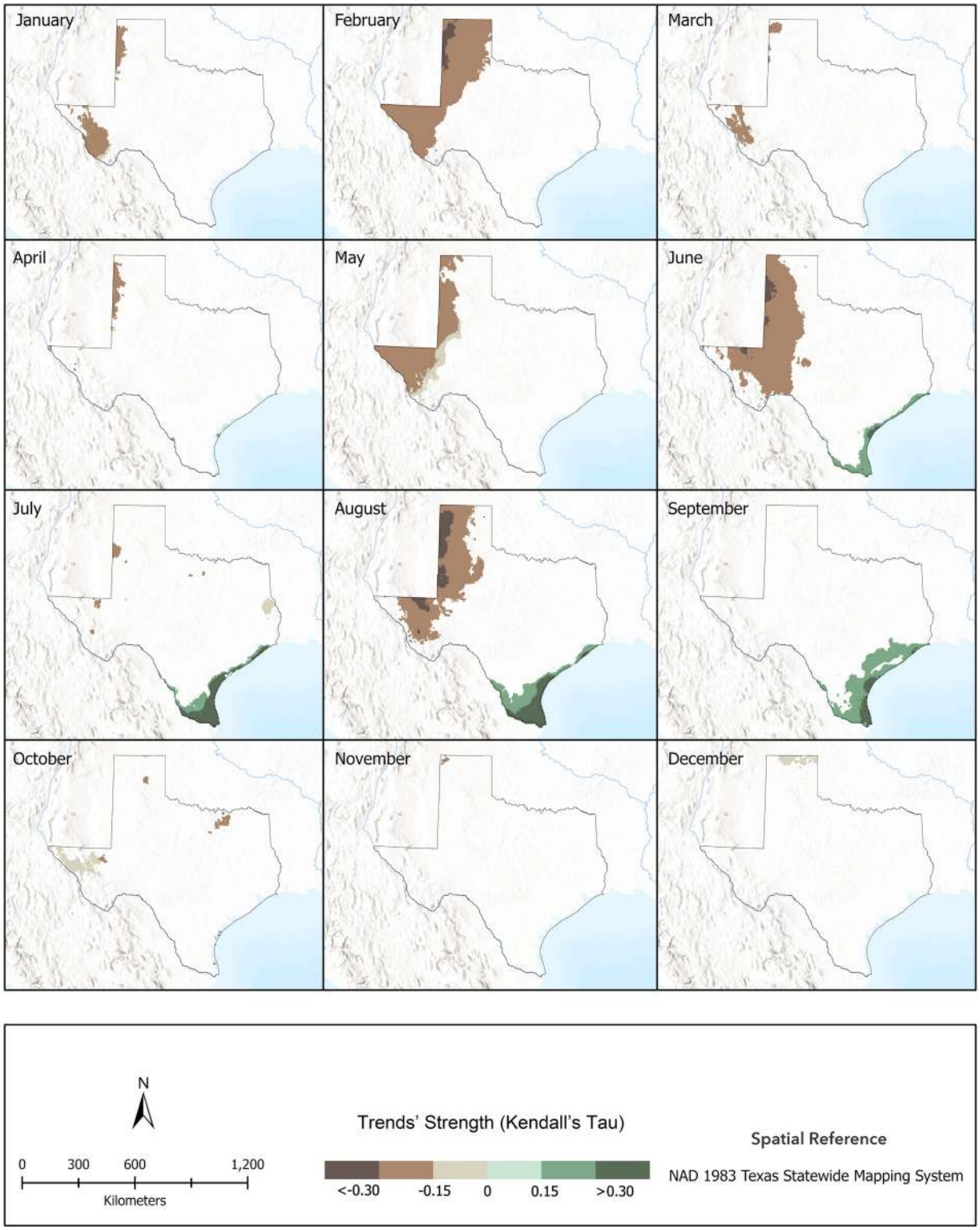

Fig. 15. Specific Humidity trend's strength in Texas, 1981–2023. Only significant trends ($p < 0.05$) are displayed.

spatial fragmentation highlights the complexity of precipitation dynamics across different times of the year and regions within the state.

4.3. Specific humidity

The spatial patterns (Figs. 14 and 15) and statistical distribution (Fig. 16) of humidity trends in Texas over the past four decades reveal a distinct northwest-southeast gradient. Negative trends are concentrated in the Far West and the Panhandle regions, particularly in February, May, June, and August, where magnitudes range from –0.34 g/kg to –2.33 g/kg and strengths from –0.06 to –0.34 Kendall's tau. Positive trends, on the other hand, are observed in the South and Southeast, particularly along the coast, from June through September, with magnitudes ranging from 1.70 g/kg to 2.44 g/kg strengths from 0.15 K to 0.30 Kendall's tau. The most pronounced changes are observed as increases in humidity over the already humid southeastern regions during the summer months.

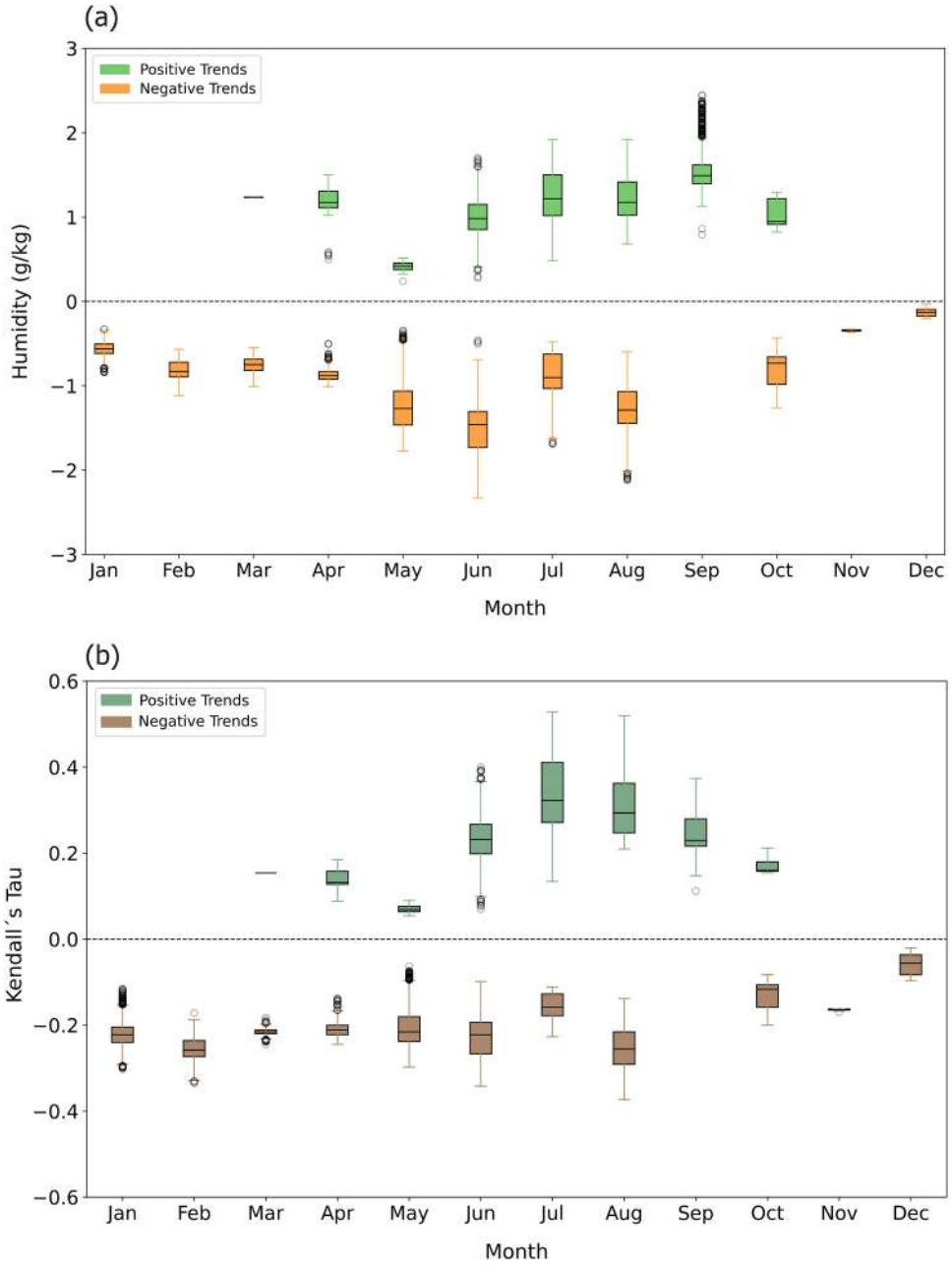

Fig. 16. Monthly a) magnitude and b) strength of specific humidity trends. Outliers are defined as values falling outside 1.5 times the interquartile range below Q1 or above Q3. See supplementary material, section A, for examples of extreme trends.

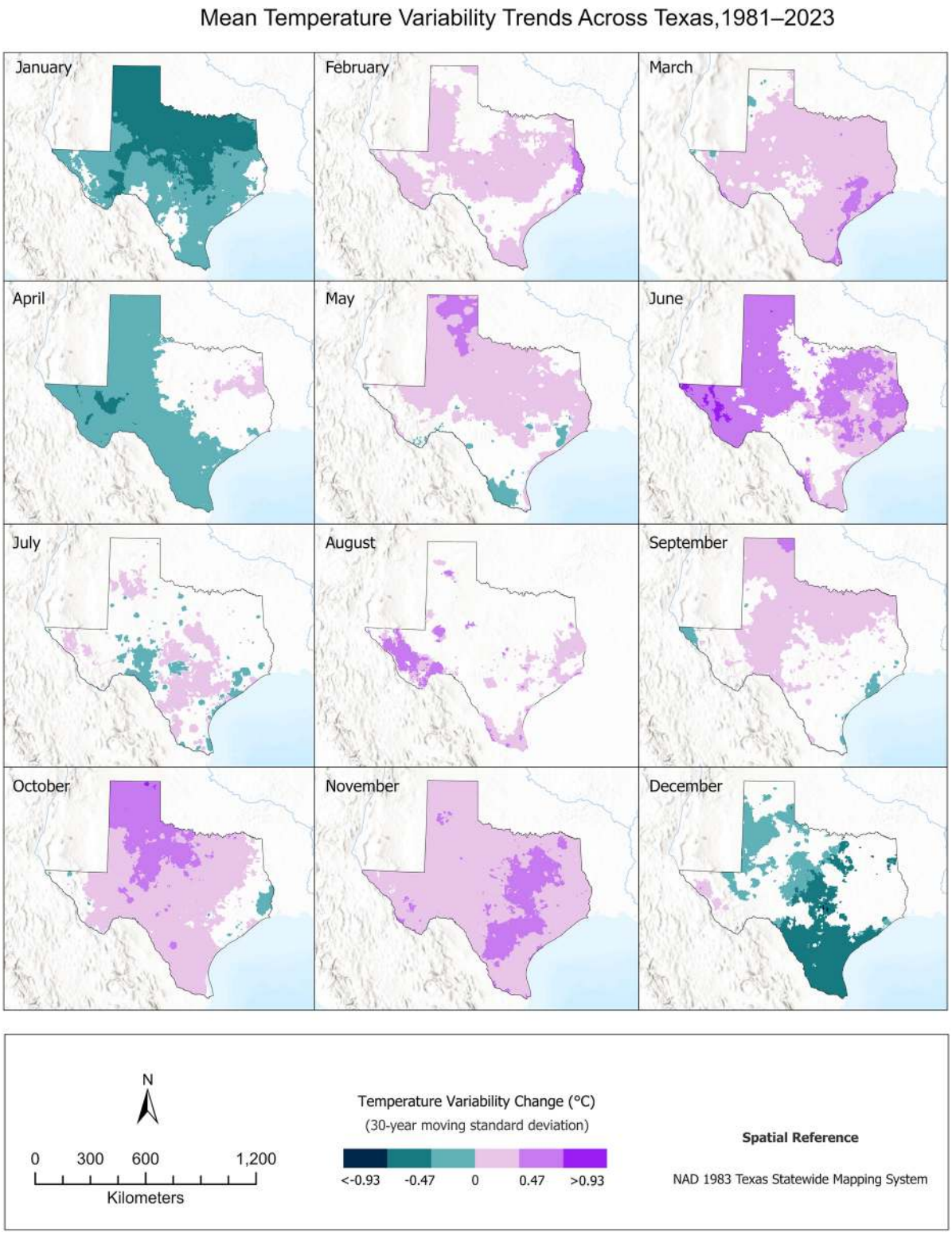

Fig. 17. Cumulative specific humidity variability changes across Texas from 1981 to 2023, based on trends in 30-year moving standard deviations of monthly mean specific humidity. Only significant trends ($p < 0.05$) are displayed.

June and August are notable for displaying distinct clusters of both increasing and decreasing trends (Figs. 14 and 15). In June, the cluster of decreasing trends exhibits a median magnitude of –1.46 g/kg and a median strength –0.22 Kendall's Tau, while the cluster of increasing trends shows a median magnitude of 0.98 g/kg and a median strength of 0.23 Kendall's Tau. The analogous negative cluster in August is shorter in magnitude (–1.29 g/kg) and stronger in strength (–0.23 Kendall's Tau), while the analogous positive cluster is larger in magnitude (1.17 g/kg) and stronger in strength (0.29 Kendall's tau). July and September also show the characteristic southeast clusters of increasing humidity trends with median magnitudes of 1.92 g/kg in both months and median strengths of 0.32 and 0.29 Kendall's Tau respectively. Significant humidity trends are largely absent across Texas during the fall months (October to December). In general, trends show greater statistical dispersion during warmer months (Fig. 16). Positive trends peak in mid to late summer, while negative trends reach their maximum in June and August. However, the latter tend to be more statistically uniform, particularly in terms of strength (Fig. 16b).

Specific monthly humidity variability displays diverse spatial and temporal patterns across Texas (Fig. 17). July and August exhibited the highest positive magnitudes of change, with increases of up to 0.63 g/kg in North Central and East Texas, indicating greater fluctuations in humidity during the summer. South Texas consistently showed decreases in variability across most months, with reductions reaching up to –1.32 g/kg, suggesting more stable and uniform humidity conditions in areas near the Gulf of Mexico. December stands out for its widespread decrease in variability, with values reaching –1.55 g/kg in South Texas. In contrast, November showed only increasing trends in variability, though with relatively low magnitudes of change. Most months showed mixed spatial patterns, with regions of both increasing and decreasing variability. This contrast highlights the spatial and seasonal complexity of humidity variability throughout the year.

5. Discussion

5.1. Climate variable trends

The primary objective of this research was to assess spatiotemporal patterns of mean temperature, total precipitation, and mean specific humidity across Texas from 1981 to 2023. Using the modified MK test and the SS estimator on gridded datasets (PRISM and GridMET), this study identified significant trends in these climate variables and quantified their strengths and magnitudes over the past four decades. The overall findings reveal that, except for temperature at the annual scale, most of Texas generally did not exhibit statistically significant trends for any of the three variables at the annual and monthly scale. Furthermore, the strengths of the observed trends, as measured by Kendall's Tau, did not exceed –/+ 0.6, indicating that the trends are not particularly strong or lack consistent monotonicity. Despite this, the regions with significant trends display distinct spatiotemporal patterns that provide valuable insights into climate changes within Texas. Moreover, the analysis of monthly variability reveals statistically significant increasing and decreasing trends that are more spatially and seasonally widespread than those observed in annual and monthly trends. These patterns highlight the growing spatial and temporal complexity of climate variability in Texas, complexity that is not captured by trends in annual or monthly values alone.

5.1.1. Temperature

Annual warming trends were observed across most of the state, with the strongest increases of up to 2.65°C occurring in Far West Texas (Figs. 3a and 4a). Monthly temperature trends exhibited notable seasonal and spatial heterogeneity (Figs. 6 and 7). Significant positive temperature trends were consistently observed throughout the year, with the most pronounced warming occurring in June, December, and September, during which 69.45 %, 36.49 %, and 31.88 % of Texas experienced increasing temperatures, respectively. The Far West, the Panhandle, East and North Central regions of Texas experienced the highest temperature increases, particularly in June and December, where changes reached up to 3.68°C with a strength of up to 0.48 Kendall's tau. These positive trends are likely to be influenced by increased solar radiation and reduced cloud cover during these months. In June, longer daylight hours and higher solar angles, combined with reduced cloud cover, enhance surface warming (Dixon and Moore, 2011). Similarly, although December marks the winter solstice and the lowest solar angle of the year, it may still receive relatively higher solar radiation compared to other winter months due to clearer skies, potentially contributing to observed warming trends (Kimmel et al., 2016).In contrast, other months experience more variable weather conditions, including increased cloud cover and precipitation, which reduce solar radiation and moderate surface temperatures (Meehl et al., 2000; Blankenau et al., 2020).

February presents a notable exception to the broader warming patterns, with localized cooling trends observed in some areas (Figs. 6 and 7). While La Niña events are generally associated with warmer and drier winter conditions across Texas, they can also influence synoptic-scale patterns, such as a northward-shifted jet stream, that intermittently allow strong Arctic air outbreaks to penetrate into the state (Albers et al., 2022). These events, although episodic, can contribute to cooler-than-average temperatures during February, especially in northern Texas and the Panhandle. This regional cooling may also be reinforced by low solar radiation and the frequent passage of intense cold fronts during this period, contributing to a distinct seasonal temperature pattern not seen in other months.

The observed increase in monthly temperature variability across most of Texas, particularly from spring through fall, suggests a shift toward more unstable and less predictable thermal conditions (Fig. 9). June stands out as a critical month, exhibiting both strong warming and a pronounced rise in variability, with cumulative increases in variability reaching 1.19 °C in Far West Texas. These dual trends indicate that the region is not only warming but also experiencing greater extremes in year-to-year temperature behavior. This pattern aligns with broader concerns about intensifying heat stress in Far West, West Central, and Panhandle regions, which fall within cold midlatitude desert, steppe, and humid subtropical climate zones (Dixon and Moore, 2011; Kimmel et al., 2016). The combination

of increasing mean temperature and variability may elevate risks related to agriculture, energy demand, and human health. In contrast, December, January, and April exhibit declining variability, suggesting greater thermal stability during those months.

The observed warming trends in Texas are consistent with broader regional and global patterns. For example, the western United States, particularly California, has experienced significant warming of up to 1.50°C in the past nine decades, which has contributed to the increasing frequency of wildfires (Cayan et al., 2008; Cordero et al., 2011). Although, the southeastern U.S. historically exhibited a "warming hole" with slower temperature increases, recent studies suggest this trend is diminishing, with warming now evident in coastal areas (Healy et al., 2023). At the global scale, temperature increases in Texas align, and in some regions exceed, the Intergovernmental Panel on Climate Change (IPCC) in 2021 reported a global average rise of 1.10°C since the pre-industrial era (Masri et al., 2022; Qiu et al., 2023). These trends reflect the broader pattern of intensified heatwaves and temperature extremes linked to anthropogenic climate change (Perkins and Lewis, 2020).

5.1.2. Precipitation

Trends in precipitation exhibit a complex pattern with smaller areas showing significant trends at both the annual (Figs. 3b and 4b) and monthly scale (Figs. 10 and 11) in comparison with temperature. The most prominent drying trends were observed in February, June, and November with 26.50 %, 24.93 %, and 15.01 % of Texas experiencing a decrease in precipitation, respectively. South, Central, and East Texas emerged as areas of concern due to their pronounced drying trends in those months. November exhibits the most extensive and intense drying in East Texas, with some areas experiencing magnitudes of change ranging from –80 to –120 mm. June showed predominantly negative precipitation trends, with decreases observed in Central Texas and the Panhandle. The average decline of 54.81 mm in this month highlights the potential for increased drought frequency and severity, as also noted by (Mishra and Singh, 2010; Wolkeba and Mekonnen, 2024). This general decline in precipitation aligns with broader trends observed in previous regional studies (Bradley and Malstaff, 2004; Dixon and Moore, 2011; Ghebreyesus and Sharif, 2021; Li, 2022). Positive trends in precipitation were sparse, with no months showing an increase in more than 5 % of the total state area. However, high magnitude outliers of increased precipitation were observed in July and August (Fig. 12a). These are primarily concentrated on the Eastern region and are likely driven by moisture influx from the Gulf of Mexico and monsoonal influences, which enhance convective activity and rainfall during the summer months. Gulf of Mexico acts as a primary moisture source for Texas, particularly in summer, when sea surface temperatures are high, and southerly winds transport moist air inland (Kimmel et al., 2016).

Significant trends in monthly precipitation variability are considerably more widespread than those in monthly totals and exhibit spatial and temporal heterogeneity that underscores the growing complexity of Texas's hydroclimate (Fig. 13). May, August, and September exhibited substantial cumulative increases in variability, up to 320 mm in some regions, particularly across Central, Eastern, and Southern Texas, pointing to intensified wet–dry fluctuations. These patterns may be associated with the increasing prevalence of convective precipitation systems during warmer months, which are characterized by short-lived, intense, and spatially localized rainfall events that amplify interannual variability (Dixon and Moore, 2011; Li et al., 2019). In contrast, February, June, and December showed widespread decreases in variability, suggesting a trend toward more stable and uniform precipitation patterns. This stability may be attributed to the dominance of large-scale atmospheric systems, such as frontal passages and winter storms, which tend to produce broader, more uniform rainfall (Dixon and Moore, 2011).

Particularly complex patterns occur in Northeast Texas, where April experienced high total precipitation changes (up to 120 mm) along with substantial cumulative changes in variability (ranging from –23 mm to 68 mm), which may reflect the combined influence of both frontal and convective systems in the region (Jiang and Yang, 2012; Kimmel et al., 2016). Similarly, parts of North, East, and Southern Texas consistently exhibit overlapping influences from both system types, resulting in spatially fragmented and seasonally erratic variability pattern (Statkewicz et al., 2021). While monthly and annual total precipitation trends remain weak or negative in many areas, the variability analysis reveals that increasing fluctuations are emerging as a key characteristic of the region's evolving rainfall regime. These findings align with global climate models indicating increased frequency and intensity of anomalous precipitation events (Sa'adi et al., 2019) and carry important implications for drought preparedness, flood risk, and long-term water resource planning, especially as surface and groundwater demands are projected to rise in the coming decades (Jiang and Yang, 2012).

The unpredictability of precipitation patterns calls for revised agricultural practices. For instance, farmers may need to transition toward drought-resistant crop varieties and implement advanced irrigation techniques to optimize water use (Bhatia et al., 2019). Additionally, changes in soil moisture levels necessitate updated land management practices to prevent erosion and maintain soil fertility (Sun et al., 2018). Climate adaptation strategies, such as improved land-use planning and investment in resilient infrastructure, will be critical in mitigating these risks (Mishra and Singh, 2010).

5.1.3. Specific Humidity

The specific humidity annual (Figs. 3c and 4c) and monthly (Figs. 14 and 15) trend analysis reveals a distinct Northwest-Southeast gradient, with notable declines in the drier western regions and marked increases in the more humid eastern areas. Positive trends were concentrated in the Southeast from June to September, with magnitudes reaching up to 2.44 g/kg. In contrast, negative trends were more prevalent in the Panhandle and Far West Texas, particularly during February, June, and August, with decreases of up to –2.33 g/kg. Decreasing trends in the west are associated with arid conditions and limited moisture availability from the Mexican Plateau. These drying are further intensified by rain shadow effects from the Rocky Mountains, which inhibit the transport of moist air from the Gulf of Mexico. Conversely, East Texas and the Gulf Coast exhibit increasing humidity trends, primarily driven by the consistent influx of the Gulf moisture, particularly during the summer months.

The monthly variability findings in specific humidity further highlight regional differences in atmospheric moisture patterns (Fig. 17). North Texas generally showed increasing humidity variability, suggesting greater fluctuations and more erratic humidity

levels. Conversely, South Texas consistently showed decreasing variability, indicating more stable and predictable humidity conditions (Fig. 17). December emerged as a month with more stable humidity patterns, while November displayed increased variability across multiple regions. The highest increases in variability were observed in July and August, especially across North-Central and East Texas, reflecting the dominance of convective activity and irregular moisture transport during the summer. These processes are known to produce short-lived, intense humidity surges that increase year-to-year fluctuations. In contrast, South Texas exhibited consistent decreases in variability across several months, particularly in December. This suggests a stabilizing influence from the Gulf of Mexico, especially during cooler months, when frontal systems and large-scale moisture advection tend to dominate (Dixon and Moore, 2011; Kimmel et al., 2016).

5.1.4. *Integrated patterns*

An integrated examination of temperature, precipitation, and specific humidity trends reveals that while annual and monthly trends are generally weak or localized across much of Texas, notable exceptions emerge both seasonally and spatially. June, in particular, stands out as a critical month, simultaneously exhibiting strong positive temperature trends, significant drying in precipitation, and both positive and negative specific humidity shifts depending on the region. These patterns reflect the compound influence of seasonal solar dynamics, convective activity, and moisture transport, all of which contribute to more pronounced and complex climate behavior during early summer.

In this context, the nature of early summer changes warrants closer attention. June showed a widespread increase in mean temperature, with an average rise of 1.80°C and a maximum increase of 3.68°C (Fig. 6). This warming was coupled with a decline in total precipitation, particularly across Central Texas, where value dropped by an average of 54.81 mm and reached a maximum decrease of 125.27 mm (Fig. 10). Mean specific humidity trends were spatially contrasting: extended declines occurred in West Texas, with an average decrease of –1.12 g/kg and a maximum of –2.33 g/kg while Southeast Texas experienced increases, averaging 1.32 g/kg and peaking at 2.44 g/kg (Fig. 14). For a closer examination, Fig. 18 illustrates both the strength and magnitude of these trends. Far West Texas experienced the strongest increasing temperature trends (>0.30 Kendall's Tau) with the highest magnitude of change (1.53°C to 3.68°C) (Fig. 8a). Central Texas exhibited clusters of moderately decreasing precipitation trends (–0.15 to –0.30 Kendall's Tau) with

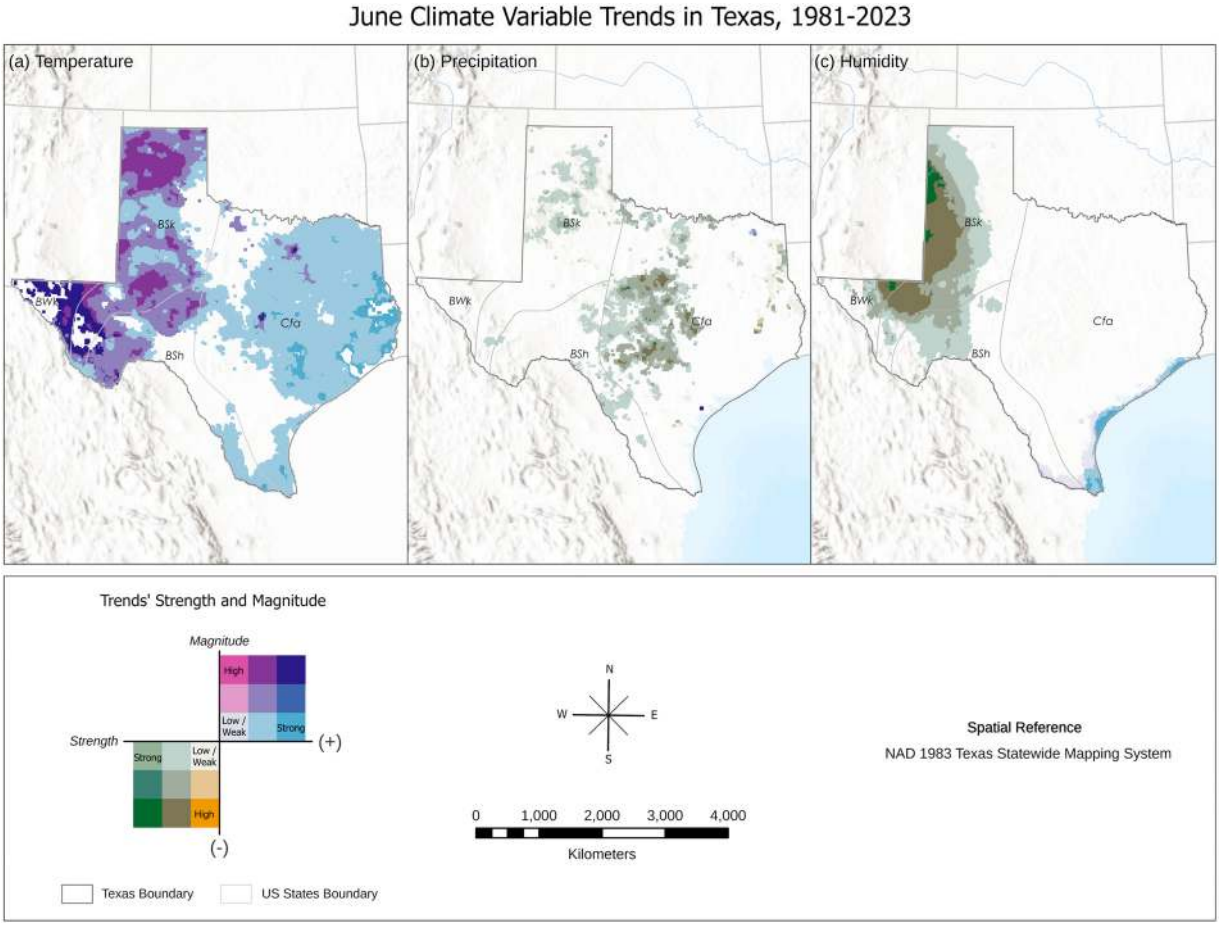

Fig. 18. June trends of (a) mean temperature, (b) total precipitation, and (c) mean specific humidity in Texas (1981–2023). Only significant trends ($p < 0.05$) are displayed. More details on how to read the map can be found in the supplementary material, section B.

high magnitudes of change (–74.74 mm to –125.27 mm), enclosed by moderately decreasing trends with moderate magnitudes of change (–55.95 mm to –74.74 mm) (Fig. 18b). West Panhandle showed the strongest decreasing specific humidity trends (<-0.30 Kendall's Tau) with the highest magnitudes of change (–1.33 g/kg to –2.33 g/kg while South and Southeast Texas mainly experienced strongly increasing specific humidity trends (>0.30 Kendall's Tau) with low magnitudes of change (0.28 g/kg to 1.78 g/kg) (Fig. 18c).

Additionally, the analysis of monthly variability across all three variables highlights broader spatial coverage and more consistent trends than those observed in monthly totals alone. An important finding is the shift toward increasingly erratic and less predictable climate conditions in some regions of Texas, especially during the warmer months. This synthesis emphasizes that understanding climate change in Texas requires not only an assessment of averages but also of the variability and interaction among climate components across space and time.

These integrated results allow for a direct evaluation of the study's guiding hypotheses. Hypothesis 1 is only weakly supported. While some localized coupling between temperature, precipitation, and specific humidity trends occur, such as in June where warming trends coincide with decreasing humidity patterns, these relationships are not consistently observed across other months or regions. Hypothesis 2 is strongly supported. Trends in interannual monthly variability are more spatially and temporally extensive than trends in monthly means or totals. These findings suggest that variability captures more nuanced shifts in climate behavior than central tendencies alone. Hypothesis 3 is supported. June emerges as the month with particularly significant and spatially extensive trends across all three variables. It exhibits the strongest warming; widespread precipitation declines and contrasting humidity changes depending. This convergence of trends reflects the compound effects of solar forcing, convective activity, and shifting moisture dynamics typical of early summer in Texas.

A recent observation by Simpson et al. (2023) in the broader U.S. Southwest suggests that humidity trends in arid regions diverge from model projections. Many of these study findings, however, align with previous research highlighting significant climatic variations specifically across Texas (Dixon and Moore, 2011; Kimmel et al., 2016; Li, 2022; Mishra et al., 2009; Mishra and Singh, 2010; Watkins and O'Connell, 2006). They also align with the broader understanding that arid and semi-arid regions are experiencing faster warming trends, potentially exacerbated by factors like wildfires and prolonged droughts. These broader regional trends emphasize that Texas's warming patterns are consistent with national climate shifts, particularly in the western U.S.

While previous research has predominantly focused on temperature and precipitation, often using station data, this study expands the scope by incorporating specific humidity trends and employing gridded datasets, which provide consistent spatial resolution and broader coverage compared to station-based analyses (Ghebreyesus and Sharif, 2021). The implications of these findings are significant for water resource management, agricultural practices, and climate adaptation strategies. The observed decrease in precipitation, particularly in Central and East Texas in June and November, poses challenges for water resource management, necessitating adaptive strategies to mitigate water scarcity. Rising temperatures and changing humidity levels could impact agricultural productivity, requiring adjustments in crop selection and irrigation practices. Shifts in precipitation and temperature patterns could significantly alter Texas' agricultural output. The need for adjusted planting schedules and water-efficient irrigation systems is increasingly evident, particularly as higher temperatures accelerate evapotranspiration rates (Condon et al., 2020; Zhou et al., 2024). Studies indicate that certain regions may need to reduce reliance on water-intensive crops or explore alternative farming techniques to maintain sustainable productivity levels (Zhang et al., 2024; Zhou et al., 2024).

Future research should prioritize incorporating additional climatic variables, such as wind speed and solar radiation, to gain deeper insights into climate dynamics. Longitudinal studies that integrate socioeconomic data to assess the long-term impacts of climatic trends on ecosystems and human systems are essential. Given the influence of large-scale climate phenomena like ENSO and the NAO on temperature and precipitation patterns, arid regions such as Texas are especially susceptible to climate variability. Therefore, future analyses should assess the influence of these climate phenomena alongside the influence of anthropogenic factors, such as land use and land cover, to provide a more comprehensive understanding of regional climate dynamics and their socio-environmental impacts.

5.2. Data limitations

Despite its strengths in topographic interpolation, the PRISM dataset exhibits known limitations, particularly in areas with complex terrain. Several studies have noted that PRISM tends to underestimate precipitation in mountainous areas, particularly in the western United States, due to sparse station coverage and challenges in capturing localized orographic effects (Daly et al., 2008). These uncertainties are reflected in cross-validation metrics such as mean absolute error and the 70 % prediction interval, which are generally higher in rugged terrain. In addition, PRISM does not explicitly account for the effects of terrain or forest canopy on surface wind speeds, which may require more advanced modeling approaches for accurate representation. Land-surface conditions such as seasonal irrigation in arid and semi-arid regions may also not be captured, potentially influencing temperature and precipitation patterns at the local scale. Furthermore, small-scale convective precipitation remains difficult to resolve due to limitations in both observational network density and the underlying atmospheric models, which may introduce inaccuracies in capturing short-lived, localized events (Abatzoglou and Brown, 2012; Valseth and Driscoll, 2021). Despite these limitations, PRISM remains one of the most reliable and widely used datasets for precipitation and temperature analysis, particularly in regions with a dense network of weather stations.

As described in Section 2, GridMET expands PRISM's spatial framework by integrating it with modeled outputs from the NLDAS to provide additional climate variables. However, this modeling approach inherits certain uncertainties from both PRISM and NLDAS, particularly in areas with complex topography or limited ground-based observational constraints. Moreover, the specific humidity data from GridMET may lack explicit bias correction, potentially introducing errors in water vapor and vapor pressure deficit estimates (Abatzoglou, 2013). While these limitations should be acknowledged, GridMET remains a valuable dataset for long-term climate monitoring and modeling due to its broad coverage and compatibility with high-resolution spatial analyses. Finally, while land use and

land cover differences were not separately controlled for, their influence is implicitly embedded in the climate data and likely contributes to localized variability in the magnitude and strength of trends.

6. Conclusion

This study aimed to investigate long-term spatiotemporal trends in annual and monthly mean temperature, total precipitation, and mean specific humidity, as well as their interannual variability at the monthly scale, across Texas from 1981 to 2023. To answer the guiding question "How have temperature, precipitation, and specific humidity—along with their interannual variability at the monthly scale—changed across space and time in Texas from 1981 to 2023?", we applied the modified MK test and SS estimator to 4-km gridded datasets from PRISM and GridMET.

Over the 43-year period, while much of Texas did not exhibit statistically significant trends in annual or monthly averages, distinct patterns emerged both spatially and seasonally. Statistically significant temperature trends were predominantly positive, with the strongest warming observed in June, particularly in Far West Texas where increases reached up to 3.68°C. Precipitation trends were largely negative, with notable declines concentrated during June and November in Central and East Texas, where maximum decreases reached –125.27 mm. Specific humidity trends revealed a clear northwest–southeast gradient, with decreases of up to –2.33 g/kg in the Panhandle and West Texas and increases of up to 1.71 g/kg near the Gulf Coast. Despite these changes, the strengths of most trends, as measured by Kendall's Tau, remained moderate to weak, not exceeding ±0.6. Still, these regional and seasonal signals offer valuable insight into the evolving climatic dynamics of the state.

Additionally, variability trends provided a deeper lens into the state's evolving climate behavior. Temperature variability has generally increased across Texas from spring through fall, especially in June and November, indicating a shift toward more erratic and less predictable conditions. Precipitation variability also increased notably in May, August, and September, particularly across Central, Eastern, and Southern Texas, pointing to intensifying wet–dry extremes. In contrast, February, June, and December displayed decreased precipitation variability, suggesting greater seasonal stability in certain regions. Specific humidity variability added another layer of complexity; while North Central and East Texas exhibited increased fluctuations in summer, South Texas consistently showed decreased variability across most months, reflecting more stable atmospheric moisture conditions near the Gulf.

These findings allowed for a direct evaluation of the study's guiding hypotheses. Hypothesis 1 was only weakly supported, as temperature, precipitation, and specific humidity trends showed limited spatial and seasonal alignment. Hypothesis 2 was strongly supported, as interannual monthly variability trends proved more spatially and temporally extensive than trends in monthly means or totals. Finally, Hypothesis 3 was supported, with June emerging as the most climatically dynamic month across all three variables. This convergence highlights the importance of early summer in shaping climate signals across Texas and demonstrates the value of integrating variability metrics into regional climate assessments.

The results also suggest that humidity levels are generally increasing in regions influenced by moisture from the Gulf of Mexico, while drier and warmer conditions are becoming more pronounced in western regions and the Panhandle, where arid air masses from the Mexican Plateau dominate. These latter regions, already characterized by water scarcity, are likely to face intensified aridification, with direct consequences for agriculture, water resource management, and regional resilience. Future research should build on these findings by examining additional climatic variables, such as wind speed and solar radiation, and socio-economic data to better assess long-term impacts on ecosystems and human systems. Exploring the influence of large-scale phenomena such as ENSO and the NAO as well as anthropogenic factors such as urbanization, land-use changes, infrastructure development, and irrigation will also enhance understanding. These insights contribute to a growing body of literature on regional climate dynamics and highlight the importance of proactive adaptation strategies to meet the challenges posed by a changing climate.

CRediT authorship contribution statement

M Shahriar Sonet: Writing – original draft, Visualization, Methodology, Formal analysis, Data curation, Conceptualization. **Yunuen Reygadas:** Writing – review & editing, Supervision, Project administration, Methodology, Investigation, Data curation, Conceptualization.

Declaration of Competing Interest

The authors declare that they have no known competing financial interests or personal relationships that could have appeared to influence the work reported in this paper.

Appendix A. Supporting information

Supplementary data associated with this article can be found in the online version at doi:10.1016/j.ejrh.2025.102539.

Data availability

Data will be made available on request.

References

Abatzoglou, J.T., 2013. Development of gridded surface meteorological data for ecological applications and modelling. Int. J. Climatol. 33 (1), 121–131. https://doi.org/10.1002/JOC.3413.

Abatzoglou, J.T., Brown, T.J., 2012. A comparison of statistical downscaling methods suited for wildfire applications. Int. J. Climatol. 32 (5), 772–780. https://doi.org/10.1002/JOC.2312.

Ahmad, I., Tang, D., Wang, T., Wang, M., Wagan, B., 2015. Precipitation trends over time using Mann-Kendall and spearman's rho tests in SWAT river basin, Pakistan. Adv. Meteorol. 2015. https://doi.org/10.1155/2015/431860.

Albers, J.R., Newman, M., Hoell, A., Breeden, M.L., Wang, Y., Lou, J., 2022. The February 2021 Cold Air Outbreak in the United States: A Subseasonal Forecast of Opportunity. Bull. Am. Meteorol. Soc. 103 (12), E2887–E2904. https://doi.org/10.1175/BAMS-D-21-0266.1.

Bhatia, N., Singh, V.P., Lee, K., 2019. Variability of extreme precipitation over Texas and its relation with climatic cycles. Theor. Appl. Climatol. 138 (1–2), 449–467. https://doi.org/10.1007/s00704-019-02840-w.

Blankenau, P.A., Kilic, A., Allen, R., 2020. An evaluation of gridded weather data sets for the purpose of estimating reference evapotranspiration in the United States. Agric. Water Manag. 242, 106376. https://doi.org/10.1016/j.agwat.2020.106376.

Bradley, R.G., Malstaff, G., 2004. Dry periods and drought events of the Edwards Plateau, Texas. In Aquifers of the Edwards Plateau. Texas Water Development Board, Austin, pp. 201–210.

Brussolo, E., Palazzi, E., Von Hardenberg, J., Masetti, G., Vivaldo, G., Previati, M., Canone, D., Gisolo, D., Bevilacqua, I., Provenzale, A., Ferraris, S., 2022. Aquifer recharge in the Piedmont Alpine zone: Historical trends and future scenarios. Hydrol. Earth Syst. Sci. 26 (2), 407–427. https://doi.org/10.5194/hess-26-407-2022.

Cayan, D.R., Maurer, E.P., Dettinger, M.D., Tyree, M., Hayhoe, K., 2008. Climate change scenarios for the California region. Clim. Change 87, 21–42.

Condon, L.E., Atchley, A.L., Maxwell, R.M., 2020. Evapotranspiration depletes groundwater under warming over the contiguous United States. Nat. Commun. 11 (1). https://doi.org/10.1038/s41467-020-14688-0.

Cordero, E.C., Kessomkiat, W., Abatzoglou, J., Mauget, S.A., 2011. The identification of distinct patterns in California temperature trends. Clim. Change 108, 357–382.

Costache, R., Hong, H., Pham, Q.B., 2020. Comparative assessment of the flash-flood potential within small mountain catchments using bivariate statistics and their novel hybrid integration with machine learning models. Sci. Total Environ. 711, 134514. https://doi.org/10.1016/J.SCITOTENV.2019.134514.

Daly, C., Halbleib, M., Smith, J.I., Gibson, W.P., Doggett, M.K., Taylor, G.H., Pasteris, P.P., 2008. Physiographically sensitive mapping of climatological temperature and precipitation across the conterminous United States. Int. J. Climatol. A J. R. Meteorol. Soc. 28 (15), 2031–2064. https://doi.org/10.1002/joc.1688.

Daly, C., Smith, J.I., Olson, K.V., 2015. Mapping atmospheric moisture climatologies across the conterminous United States. PLoS ONE 10 (10). https://doi.org/10.1371/journal.pone.0141140.

Daly, C., Doggett, M.K., Smith, J.I., Olson, K.V., Halbleib, M.D., Dimcovic, Z., Ryan, A.D., 2021. Challenges in observation-based mapping of daily precipitation across the conterminous United States. J. Atmos. Ocean. Technol. 38 (11), 1979–1992. https://doi.org/10.1175/JTECH-D-21-0054.1.

Dixon, R.W., Moore, T.W., 2011. Trend detection in Texas temperature and precipitation. Southwest. Geogr. 15, 80–103.

El-Nesr, M.N., Abu-Zreig, M.M., Alazba, A.A., 2010. Temperature trends and distribution in the Arabian Peninsula. Am. J. Environ. Sci. 6 (2), 191–203. http://www.scipub.org/fulltext/ajes/ajes62191-203.pdf.

Ghebreyesus, D., Sharif, H.O., 2021. Time series analysis of monthly and annual precipitation in the state of Texas using high-resolution radar products. Water 13 (7), 982. https://doi.org/10.3390/w13070982.

Gocic, M., Trajkovic, S., 2013. Analysis of changes in meteorological variables using Mann-Kendall and Sen's slope estimator statistical tests in Serbia. Glob. Planet. Change 100, 172–182. https://doi.org/10.1016/j.gloplacha.2012.10.014.

Hamed, K.H., Rao, A.R., 1998. A modified Mann-Kendall trend test for autocorrelated data. J. Hydrol. 204 (1–4), 182–196. https://doi.org/10.1016/S0022-1694(97)00125-X.

Hao, Z., Singh, V., 2013. Entropy-based method for extreme rainfall analysis in Texas. J. Geophys. Res. Atmospheres 118 (2), 263–273. https://doi.org/10.1029/2011JD017394.

Healy, J.P., Yazdi, M.D., Wei, Y., Qiu, X., Shtein, A., Dominici, F., Shi, L., Schwartz, J.D., 2023. Seasonal Temperature Variability and Mortality in the Medicare Population. Environ. Health Perspect. 131 (7). https://doi.org/10.1289/EHP11588.

Hooshyar, M., Wagner, C.E., Baker, R.E., Metcalf, C.J.E., Grenfell, B.T., Porporato, A., 2020. Cyclic epidemics and extreme outbreaks induced by hydro-climatic variability and memory. J. R. Soc. Interface 17 (171), 20200521. https://doi.org/10.1098/rsif.2020.0521.

Huan, H., Wang, J., Teng, Y., 2012. Assessment and validation of groundwater vulnerability to nitrate based on a modified DRASTIC model: a case study in Jilin City of northeast China. Sci. Total Environ. 440, 14–23. https://doi.org/10.1016/j.scitotenv.2012.08.037.

Jiang, X., Yang, Z.L., 2012. Projected changes of temperature and precipitation in Texas from downscaled global climate models. Clim. Res. 53 (3), 229–244. https://doi.org/10.3354/cr01093.

Karaburun, A., Demirci, A., Kara, F., 2011. Analysis of spatially distributed annual, seasonal and monthly temperatures in Istanbul from 1975 to 2006. World Appl. Sci. J. 12 (10), 1662–1675.

Kendall, M.G., 1948. Rank Correl. Methods.

Kimmel, T.M., Nielsen-Gammon, J., Rose, B., Mogil, H.M., 2016. The Weather and Climate of Texas: A Big State With Big Extremes. Weatherwise 69 (5), 25–33. https://doi.org/10.1080/00431672.2016.1206446.

Kottek, M., Grieser, J., Beck, C., Rudolf, B., Rubel, F., 2006. World map of the Köppen-Geiger climate classification updated. Meteorol. Z. 15 (3), 259–263. https://doi.org/10.1127/0941-2948/2006/0130.

Li, Y., 2022. Century-long changing climate of Texas: the spatial-temporal variability and trends of temperature and precipitation. Int. J. Glob. Warm. 27 (1), 102–122. https://doi.org/10.1504/IJGW.2022.122798.

Li, Z., Li, X., Wang, Y., Quiring, S.M., 2019. Impact of climate change on precipitation patterns in Houston, Texas, USA. Anthropocene 25, 100193. https://doi.org/10.1016/j.ancene.2019.100193.

Liyew, C.M., Meo, R., Ferraris, S., Di Nardo, E., 2024a. Analysis of Diurnal Air Temperature Trends and Pattern Similarities in Highland and Lowland Stations of Italy and UK. Int. J. Climatol. https://doi.org/10.1002/joc.8643.

Liyew, C.M., Di Nardo, E., Meo, R., Ferraris, S., 2024b. Identifying time patterns of highland and lowland air temperature trends in Italy and the UK across monthly and annual scales. Adv. Stat. Climatol. Meteorol. Oceanogr. 10 (2), 173–194. https://doi.org/10.5194/ascmo-10-173-2024.

Lu, Y., He, T., Xu, X., Qiao, Z., 2021. Investigation the robustness of standard classification methods for defining urban heat islands. IEEE J. Sel. Top. Appl. Earth Obs. Remote Sens. 14, 11386–11394. https://doi.org/10.1109/JSTARS.2021.3124558.

Masri, S., Jin, Y., Wu, J., 2022. Compound Risk of Air Pollution and Heat Days and the Influence of Wildfire by SES across California, 2018–2020: Implications for Environmental Justice in the Context of Climate Change. Climate 10 (10), 145. https://doi.org/10.3390/CLI10100145/S1.

Meehl, G.A., Zwiers, F., Evans, J., Knutson, T., Mearns, L., Whetton, P., 2000. Trends in extreme weather and climate events: issues related to modeling extremes in projections of future climate change. Bull. Am. Meteorol. Soc. 81 (3), 427–436. https://doi.org/10.1175/1520-0477(2000)0812.3.CO;2.

Mishra, A.K., Singh, V.P., 2010. Changes in extreme precipitation in Texas. J. Geophys. Res. Atmospheres 115 (D14). https://doi.org/10.1029/2009JD013398.

Mishra, A.K., Özger, M., Singh, V.P., 2009. An entropy-based investigation into the variability of precipitation. J. Hydrol. 370 (1–4), 139–154. https://doi.org/10.1016/j.jhydrol.2009.03.006.
Neyestani, A., Karami, K., Gholami, S., 2022. Exploring the possible linkage between the precipitation and temperature over Iran and their association with the large-scale circulations: Cumulative spectral power and wavelet coherence approaches. Atmos. Res. 274, 106187. https://doi.org/10.1016/j.atmosres.2022.106187.
North, D.C., 1995b. The new institutional economics and third world development. In The New Institutional Economics and Third World Development. Routledge, pp. 31–40.
North, D.C., 1995a. Five propositions about institutional change. Explain. Soc. Inst. 99–116.
Perkins, S.E., Lewis, S.C., 2020. Increasing trends in regional heatwaves. Nat. Commun. 2020 11:1, 11 (1), 1–8. https://doi.org/10.1038/s41467-020-16970-7.
Qiu, R., Han, G., Li, S., Tian, F., Ma, X., Gong, W., 2023. Soil moisture dominates the variation of gross primary productivity during hot drought in drylands. Sci. Total Environ. 899. https://doi.org/10.1016/j.scitotenv.2023.165686.
Rajagopalan, B., Nowak, K., Prairie, J., Hoerling, M., Harding, B., Barsugli, J., Udall, B., 2009. Water supply risk on the Colorado River: Can management mitigate? Water Resour. Res. 45 (8). https://doi.org/10.1029/2008WR007652.
Reygadas, Y., Spera, S.A., Salisbury, D.S., 2023. Effects of deforestation and forest degradation on ecosystem service indicators across the Southwestern Amazon. Ecol. Indic. 147, 109996. https://doi.org/10.1016/j.ecolind.2023.109996.
Russell, R.J., 1945. Climates of Texas. Ann. Assoc. Am. Geogr. 35 (2), 37–52. https://doi.org/10.1080/00045604509357268.
Sa'adi, Z., Shahid, S., Ismail, T., Chung, E.S., Wang, X.J., 2019. Trends analysis of rainfall and rainfall extremes in Sarawak, Malaysia using modified Mann–Kendall test. Meteorol. Atmos. Phys. 131 (3), 263–277. https://doi.org/10.1007/s00703-017-0564-3.
Sagarika, S., Kalra, A., Ahmad, S., 2014. Evaluating the effect of persistence on long-term trends and analyzing step changes in streamflows of the continental United States. J. Hydrol. 517, 36–53. https://doi.org/10.1016/j.jhydrol.2014.05.002.
Sawyer, P., Stephen, H., 2014. The Big Pine Creek watershed and climate change: A trend analysis of Landsat surface reflectance and PRISM datasets over the last 3 decades. Adv. Space Res. 54 (1), 37–48. https://doi.org/10.1016/j.asr.2014.03.007.
Schmandt, J., North, G.R., Clarkson, J., 2011. The Impact of Global Warming on Texas. University of Texas Press.
Schreiner-McGraw, A.P., Ajami, H., 2022. Combined impacts of uncertainty in precipitation and air temperature on simulated mountain system recharge from an integrated hydrologic model. Hydrol. Earth Syst. Sci. 26 (4), 1145–1164. https://doi.org/10.5194/hess-26-1145-2022.
Sharma, C.S., Panda, S.N., Pradhan, R.P., Singh, A., Kawamura, A., 2016. Precipitation and temperature changes in eastern India by multiple trend detection methods. Atmos. Res. 180, 211–225. https://doi.org/10.1016/j.atmosres.2016.04.019.
Simpson, I.R., McKinnon, K.A., Kennedy, D., Lawrence, D.M., Lehner, F., Seager, R.I., 2023. Obs. humidity Trends Dry. Reg. Contradict Clim. Models. https://doi.org/10.1073/pnas.
Some'e, B.S., Ezani, A., Tabari, H., 2012. Spatiotemporal trends and change point of precipitation in Iran. Atmos. Res. 113, 1–12. https://doi.org/10.1016/j.atmosres.2012.04.016.
Statkewicz, M.D., Talbot, R., Rappenglueck, B., 2021. Changes in precipitation patterns in Houston, Texas. Environ. Adv. 5, 100073. https://doi.org/10.1016/j.envadv.2021.100073.
Sun, A.Y., Xia, Y., Caldwell, T.G., Hao, Z., 2018. Patterns of precipitation and soil moisture extremes in Texas, US: A complex network analysis. Adv. Water Resour. 112, 203–213. https://doi.org/10.1016/j.advwatres.2017.12.019.
Theil, H., 1950. A rank-invariant method of linear and polynomial regression analysis. Indag. Math. 12 (85), 173.
Valseth, K.J., Driscoll, D.G., 2021. Characterization of factors affecting groundwater levels in and near the former Lake Traverse Indian Reservation, South Dakota, water years 1956–2017. Sci. Investig. Rep. 2020–5151, 1–64. https://doi.org/10.3133/SIR20205151.
Watkins, D., O'Connell, S., 2006. Teleconnections and disconnections in Central Texas: A guide for water managers. In: Garbrecht, J.D., Piechota, T.C. (Eds.), Climate variations, climate change, and water resources engineering. American Society of Civil Engineers, Reston,USA, pp. 103–114.
Wolkeba, F.T., Mekonnen, M.M., 2024. Evaluation of gridded precipitation data in water availability modeling in CONUS. J. Hydrol. 628, 130575. https://doi.org/10.1016/j.jhydrol.2023.130575.
Yunling, H., Yiping, Z., 2005. Climate change from 1960 to 2000 in the Lancang River Valley, China. Mt. Res. Dev. 25 (4), 341–348. https://doi.org/10.1659/0276-4741(2005)025[0341:CCFTIT]2.0.CO;2.
Zhang, L., Yu, Y., Guo, Z., Ding, X., Zhang, J., Yu, R., 2024. Investigating agricultural water sustainability in arid regions with Bayesian network and water footprint theories. Sci. Total Environ. 951. https://doi.org/10.1016/j.scitotenv.2024.175544.
Zhou, J., Luo, Y., Wang, J., Dou, J., Wang, L., Shi, W., Zhang, D., Wei, W., Zhu, G., 2024. Impacts of planting structure adjustment on water saving in the Shiyang River Basin of Arid Region. Sci. Rep. 14 (1). https://doi.org/10.1038/s41598-024-80105-x.